nature neuroscience

Segregated cholinergic transmission modulates dopamine neurons integrated in distinct functional circuits

Daniel Dautan[1–3], Albert S Souza[1,8], Icnelia Huerta-Ocampo[1,3], Miguel Valencia[3–5], Maxime Assous[3], Ilana B Witten[6], Karl Deisseroth[7], James M Tepper[3], J Paul Bolam[1], Todor V Gerdjikov[2] & Juan Mena-Segovia[1,3]

Dopamine neurons in the ventral tegmental area (VTA) receive cholinergic innervation from brainstem structures that are associated with either movement or reward. Whereas cholinergic neurons of the pedunculopontine nucleus (PPN) carry an associative/motor signal, those of the laterodorsal tegmental nucleus (LDT) convey limbic information. We used optogenetics and *in vivo* juxtacellular recording and labeling to examine the influence of brainstem cholinergic innervation of distinct neuronal subpopulations in the VTA. We found that LDT cholinergic axons selectively enhanced the bursting activity of mesolimbic dopamine neurons that were excited by aversive stimulation. In contrast, PPN cholinergic axons activated and changed the discharge properties of VTA neurons that were integrated in distinct functional circuits and were inhibited by aversive stimulation. Although both structures conveyed a reinforcing signal, they had opposite roles in locomotion. Our results demonstrate that two modes of cholinergic transmission operate in the VTA and segregate the neurons involved in different reward circuits.

© 2016 Nature America, Inc. All rights reserved.

Dopamine neurons (DA) of the ventral tegmental area (VTA) have been implicated in goal-directed behaviors and reinforcement learning[1]. Their discharge mode changes from tonic to phasic in response to sensory events that predict a reward outcome[2]. This phasic activation produces synchronous bursts[3] and encodes a prediction error signal that is crucial for reinforcement learning[4]. Thus, the switch in the firing mode of DA neurons, which is triggered by excitatory drive, is critical for the expression of reward-oriented behavior[5].

The VTA receives excitatory inputs from several regions, including the prefrontal cortex, amygdala, lateral hypothalamus, subthalamic nucleus and mesopontine tegmentum in the brainstem[6]. Although all of these afferent systems provide a glutamatergic input, the mesopontine tegmentum, composed of the pedunculopontine nucleus (PPN) and the laterodorsal tegmental nucleus (LDT), also provides the main source of cholinergic innervation of DA neurons[7]. Previous reports have shown that glutamatergic mechanisms following PPN stimulation are involved, which lead to increases in the number of DA neurons bursting[8,9]. Similarly, activating a predominantly glutamatergic projection from the LDT produces burst firing in DA neurons[10] and elicits conditioned place preference in behaving rodents[11]. However, less clear is the influence of cholinergic afferents over the activity of DA neurons *in vivo*. Nicotinic[12] and muscarinic acetylcholine receptors are widely expressed in the VTA and their activation in brain slices causes depolarization[13,14] and burst firing[15] in DA neurons. Furthermore, behavioral experiments have consistently shown a prominent role for VTA acetylcholine receptors in goal-directed behavior and addiction[16], presumably through the activation of DA neurons[17]. It is therefore likely that cholinergic afferents, derived from the mesopontine tegmentum, are involved in tuning the activity of DA neurons in the VTA.

PPN and LDT share similar connections and neurochemistry, but differ in the functional networks to which they contribute. Whereas PPN is connected to sensorimotor and associative structures[18], as well as those involved in the regulation of arousal[19], the LDT is connected to limbic systems[20]. Because DA neurons are heterogeneous in terms of their firing properties, connectivity and functionality[21–26], it is likely that brainstem cholinergic pathways produce different effects in the VTA and differentially affect subpopulations of DA neurons.

To address these issues, we characterized the innervation of the VTA by PPN and LDT cholinergic neurons by retrograde and anterograde labeling. Using an optogenetic approach in transgenic rats that expresses Cre recombinase under the choline acetyltransferase (ChAT) promoter (ChAT::Cre^{+})[27], combined with *in vivo* juxtacellular single-cell recording and labeling, micro-iontophoretic drug delivery, and retrograde labeling, we characterized the effect of the activation of PPN or LDT cholinergic afferents on the spontaneous activity of identified DA and non-DA neurons in the VTA. We then identified the targets of a subset of DA neurons and correlated their responses to cholinergic modulation with the functional circuit in which they participate. Finally, we characterized the functional role of these cholinergic afferents in a reward-related behavior and in locomotion.

RESULTS

Cholinergic neurons modulate the activity of VTA neurons

We first made deposits of two retrograde tracers in the VTA (rostral and caudal, $n = 4$ rats) to determine the topographical organization of

[1]MRC Anatomical Neuropharmacology Unit, Department of Pharmacology, University of Oxford, Oxford, UK. [2]School of Psychology, University of Leicester, Leicester, UK. [3]Center for Molecular and Behavioral Neuroscience, Rutgers University, Newark, New Jersey, USA. [4]CIMA, Universidad de Navarra, Pamplona, Spain. [5]diSNA, Navarra Institute for Health Research, Pamplona, Spain. [6]Princeton Neuroscience Institute, Princeton, New Jersey, USA. [7]Department of Psychiatry, Stanford University, Stanford, California, USA. [8]Present address: Universidade Federal de Mato Grosso do Sul, Brazil. Correspondence should be addressed to J.M.-S. (juan.mena@rutgers.edu).

Received 29 March; accepted 27 May; published online 27 June 2016; doi:10.1038/nn.4335

the brainstem cholinergic innervation of the VTA. Cholinergic neurons of the caudal PPN and LDT innervated both rostral and caudal regions of the VTA, arising from similar numbers of cholinergic neurons in PPN and LDT (**Supplementary Fig. 1** and **Supplementary Table 1**). Next, we used Chat::Cre$^+$ rats. We injected into the PPN or LDT an AAV vector that incorporates a transgene encoding a fluorescent reporter (enhanced yellow fluorescent protein, eYFP) and a light-activated ion channel (channelrhodopsin-2, ChR2) (AAV2-EF1a-DIO-hChR2-eYFP; **Figs. 1a** and **2a**). Appropriate controls were used to verify the vector specificity for cholinergic neurons both in the brainstem (n = 5 rats) and other brain regions (n = 3 rats) using a vector that encodes only the fluorescent reporter (**Supplementary Fig. 2**, **Supplementary Table 2**, and Online Methods). In addition, we injected the same vector in each cholinergic cell group across the brain (Ch1–Ch8, n = 3 rats per group) and confirmed that only PPN and LDT provided cholinergic innervation of the VTA (**Supplementary Fig. 3**). In both PPN- and LDT-injected rats, we detected fluorescently labeled axons in the VTA, the borders of which were defined by the distribution of tyrosine-hydroxylase-immunopositive (TH$^+$) neurons (**Figs. 1b** and **2b**). Labeled axons were mapped across the full extent of the VTA and revealed a relatively homogeneous distribution whether they were derived from the PPN or LDT (n = 3 rats each), although LDT axons had a greater overall length than PPN axons (albeit not significant; t = 1.29, two-tailed t test, P = 0.266; **Supplementary Fig. 4**) and showed an area of higher density in the dorsal part of the parabrachial pigmented area (**Figs. 1c** and **2c**). Consecutive sections were processed for electron microscopy to characterize the synapses formed by YFP-expressing cholinergic axons. Gray's type 1 synapses (asymmetrical) were formed by PPN cholinergic axons with DA dendrites, whereas LDT cholinergic axons formed asymmetrical synapses with both DA and non-DA dendrites (40 and 60%, respectively). In contrast, Gray's type 2 synapses (symmetrical) from both structures were formed predominantly in non-DA structures (80% for PPN and 100% for LDT). Furthermore, the synapses derived from the PPN made contacts with a larger proportion of DA processes (**Figs. 1d** and **2d**), whereas those derived from the LDT showed a greater preference for non-DA processes (**Figs. 1e** and **2e**). The combined results from the anatomical characterization therefore reveal that cholinergic axons originating in the PPN and LDT are intermingled in the VTA and contact both DA and non-DA neurons. In addition, although the number of VTA-projecting cholinergic neurons was similar between PPN and LDT, the axonal mapping indicates that the latter has a higher level of collateralization, which gives rise to a larger number of synaptic contacts with non-DA neurons.

Next we tested the effect of optogenetic stimulation of the brainstem cholinergic axons on neurochemically identified VTA neurons recorded *in vivo* and juxtacellularly labeled. Following the *post hoc* histological identification of the recorded neurons, we classified them as DA (TH$^+$) or non-DA (TH$^-$) (**Figs. 1f,g** and **2f,g**). The firing rate and pattern of each neuron during light stimulation was compared with their firing characteristics during the preceding baseline period (10 s). Two to four trials were carried out for each neuron and combined to calculate the average response (**Supplementary Fig. 5** and Online Methods). Following light stimulation of

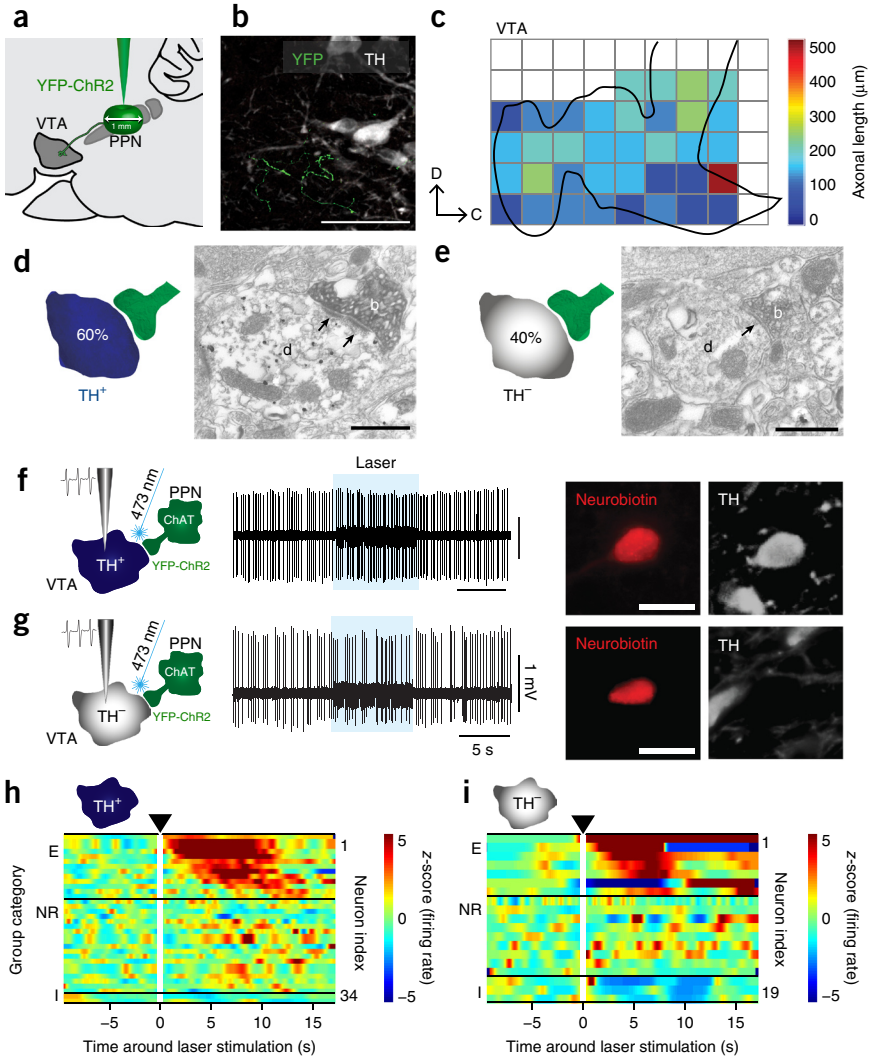

Figure 1 Optogenetic activation of PPN cholinergic axons modulates DA and non-DA neurons of the VTA. (**a**) An AAV vector (AAV2-DIO-EF1a-eYFP-ChR2) was injected into the caudal PPN of ChAT::Cre$^+$ rats (n = 22 rats). (**b**,**c**) YFP-positive axons were detected in the VTA (**b**) and mapped using 250-µm^2 grids (n = 6 rats; **c**). D, dorsal; C, caudal. (**d**,**e**) PPN cholinergic axons (n = 10 boutons (b) in n = 5 rats) made synaptic contacts (arrows) with both TH$^+$ and TH$^-$ dendrites (d). (**f**) Individual TH$^+$ neurons (n = 34 neurons in 22 rats) were recorded *in vivo* during optogenetic stimulation of PPN axons (8 s, 10 Hz, 50-ms pulses) and were subsequently labeled with neurobiotin. (**g**) The same protocol was followed for TH$^-$ neurons (n = 19 neurons in 22 rats). (**h**) Normalized firing rate (z-score along the whole trial period) for each TH$^+$ neuron around the laser stimulation in the VTA showing three categories of neurons: excited (E, 38%), non-responsive (NR, 56%) and inhibited (I, 6%) (cluster-based permutation test, 200 permutations). (**i**) Normalized firing rates of TH$^-$ neurons show similar proportions in each group in relation to their response (E, 37%; NR, 47%; I, 16%). Scale bars represent 70 µm (**b**), 0.5 µm (**d**,**e**) and 50 µm (**f**,**g**).

© 2016 Nature America, Inc. All rights reserved.

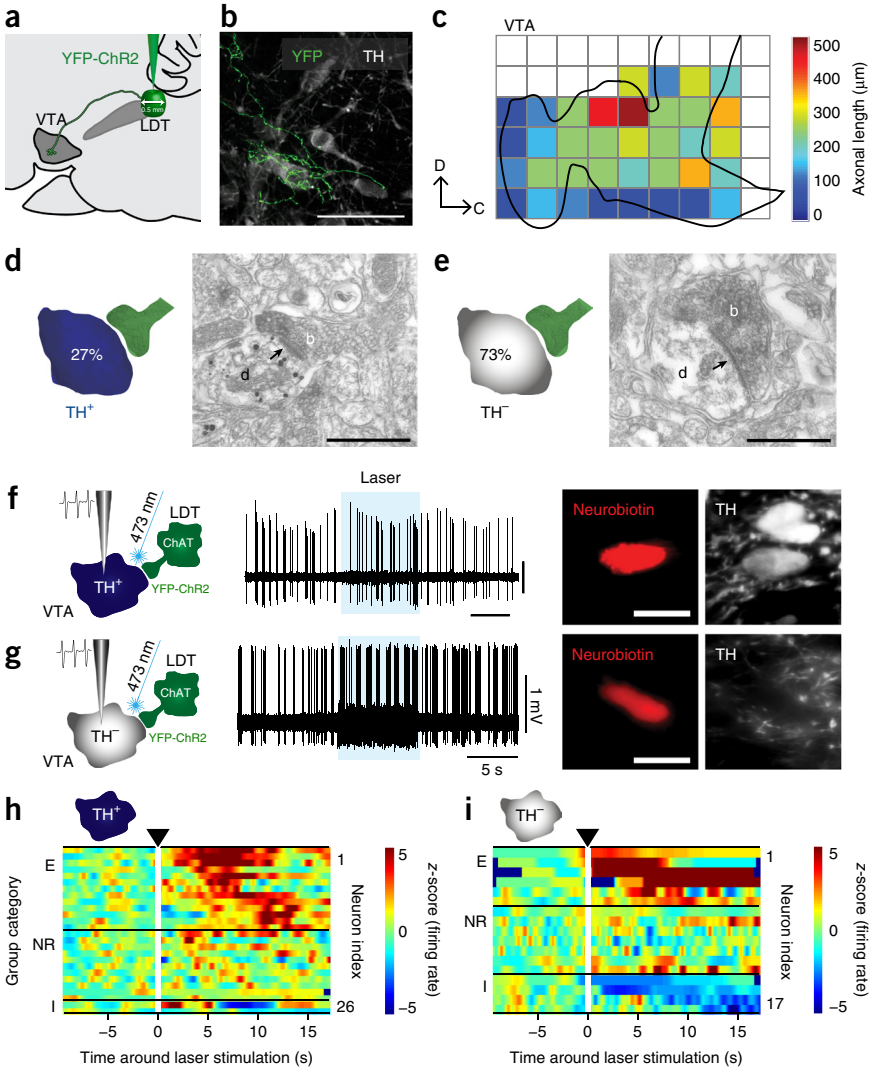

Figure 2 Optogenetic activation of LDT cholinergic axons modulates DA and non-DA neurons of the VTA. (**a**) Virus injections were delivered into the LDT (n = 19 rats). (**b**) YFP-positive axons were observed more frequently than in PPN-injected animals (n = 6 rats). (**c**) The total axonal length was higher for the LDT, suggesting a higher level of collateralization (n = 6 rats; **Supplementary Fig. 3c**). (**d**,**e**) LDT cholinergic axons (n = 11 boutons (b) in n = 5 rats) made synaptic contacts (arrows) with TH⁻ processes more often than with TH⁺ processes (d, dendrite). (**f**,**g**) Protocol for recording, stimulation (8 s, 10 Hz, 50-ms pulses) and labeling of TH⁺ (n = 26) and TH⁻ (n = 17) neurons (in 19 rats). (**h**) Neurons were separated into three categories according to their responses to the laser stimulation: excited (E, 50%), non-responsive (NR, 42%), and inhibited (I, 8%) (cluster-based permutation test, 200 permutations). (**i**) There was more variability in the responses of TH⁻ neurons to the LDT stimulation (E, 35%; NR, 41%; I, 24%). Scale bars represent 70 µm (**b**), 0.5 µm (**d**,**e**) and 50 µm (**f**,**g**).

cholinergic axons from either the PPN or LDT, we observed both excitatory and inhibitory responses in both DA and non-DA neurons, although the proportions varied slightly. No responses were observed when cholinergic neurons were transduced with just the fluorescent reporter (**Supplementary Fig. 6**). Stimulation of axons from the PPN produced predominantly excitation in responding DA neurons (**Fig. 1h**), whereas only a small fraction showed inhibition. This activation was maintained throughout the laser stimulation. The excitation of responding non-DA neurons followed similar patterns of activation during the stimulation period; however, a larger proportion of non-DA neurons were inhibited (**Fig. 1i**). The stimulation of LDT cholinergic axons also produced predominantly excitation in responding DA neurons, but the proportion of responding neurons was larger than that following PPN axon stimulation (**Fig. 2h**). In contrast with PPN axon stimulation, we observed a proportion of 'late-responding' neurons whose firing rate increased once the light stimulation stopped. The stimulation effects of LDT cholinergic axons on non-DA neurons were more variable: the excitation was not as prominent as for PPN axon stimulation, and a slightly larger proportion of non-DA neurons were inhibited (**Fig. 2i**).

The activation of DA neurons showed a slow response that increased as a function of the number of pulses and reached its maximum toward the end of the light-stimulation period (**Fig. 3**). These dynamics were observed following both PPN- (**Fig. 3a**) and LDT-cholinergic axon stimulation (**Fig. 3b**), but the magnitude of the response was slightly greater for the PPN axon stimulation, although not significant. This contrasts with short-latency responses that were observed in nigral neurons following electrical stimulation of the PPN output[9,28,29]. In a separate set of experiments, we tested the effects of *in vivo* electrical stimulation of the PPN and LDT region on identified VTA DA and non-DA neurons. Consistent with previous reports, we observed short-latency excitatory and inhibitory responses in DA

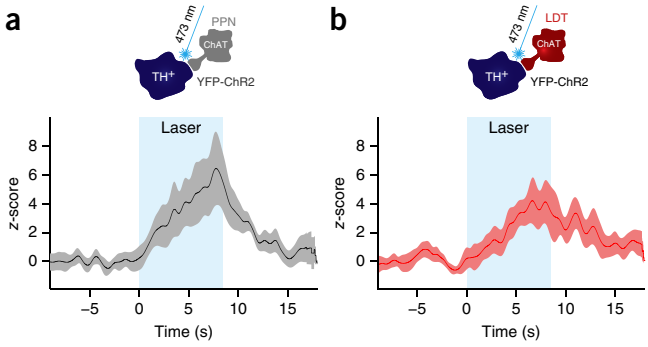

Figure 3 Activation of cholinergic axons produces a slow and robust excitation of DA neurons. (**a**,**b**) The normalized firing rate of all TH⁺ neurons that were excited by the laser stimulation showed a similar slow modulation when cholinergic axons of either PPN (**a**; n = 15 neurons in 22 rats) or LDT (**b**; n = 15 neurons in 19 rats) were stimulated. The responses following PPN cholinergic axon stimulation were greater in magnitude, and no significant differences were observed (cluster-based permutation test, P = 0.715; 200 permutations). Data are depicted as mean ± confidence interval (CI).

© 2016 Nature America, Inc. All rights reserved.

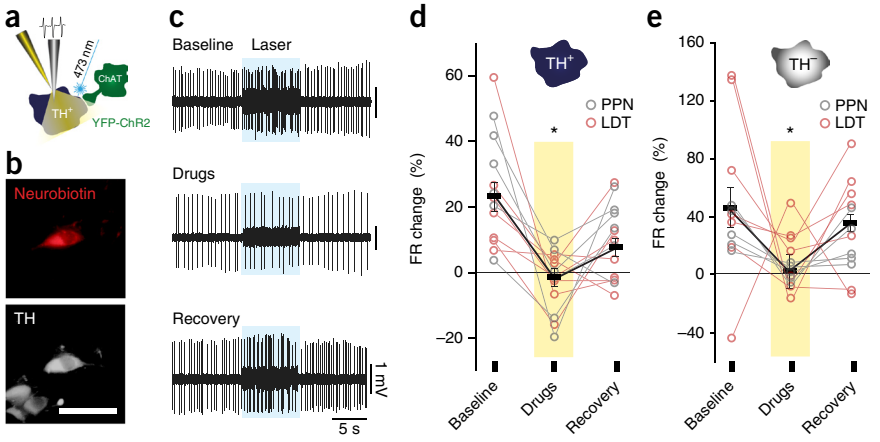

Figure 4 Cholinergic antagonists block the response to laser stimulation in DA and non-DA neurons. (**a**) Individual TH$^+$ and TH$^-$ neurons were recorded *in vivo* during optogenetic stimulation of PPN axons and local micro-iontophoretic administration of nicotinic and muscarinic antagonists (20 mM methyllycaconitine, 40 mM dihydro-β-erythroidine, 40 mM atropine and 100 μM mecamylamine; $n = 5$ rats). (**b**) Neurons were subsequently labeled with neurobiotin and their neurochemical profile was identified ($n = 14$ TH$^+$, $n = 12$ TH$^-$ neurons). (**c**) Example of a neuron that was recorded during a baseline response to the optogenetic activation of LDT cholinergic axons (see group data in **d**,**e**). Following the iontophoretic application of the acetylcholine antagonist cocktail, the same laser stimulation failed to produce a response, but the responsiveness to the laser stimulation recovered following drug wash-out (2 min after). (**d**,**e**) Excitatory responses to laser stimulation of both PPN and LDT cholinergic axons were blocked in DA ($n = 14$ of 14 neurons; $F_{1,12} = 21.3$, $P = 0.0006$, two-way mixed ANOVA) and non-DA ($n = 12$ of 12 neurons; $F_{1,9} = 20.26$, $P = 0.001$, two-way mixed ANOVA) neurons following the administration of acetylcholine antagonist cocktail and recovered following wash-out. No significant effects in the axon source (PPN/LDT) factor or in the interaction (stimulation x source) were observed. Bars represent mean ± s.e.m. *$P < 0.05$. Scale bar represents 50 μm (**b**).

© 2016 Nature America, Inc. All rights reserved.

($n = 12$ neurons) and non-DA neurons ($n = 4$ neurons) in the VTA ($n = 5$ rats; **Supplementary Fig. 7**). This suggests that electrically stimulating the output of the PPN and LDT leads to a combined response that is mediated by glutamatergic, GABAergic and cholinergic transmission, whereas the optogenetic manipulation dissects out the cholinergic terminals.

To ensure that the responses to light stimulation were mediated by released acetylcholine, in a separate set of experiments, we attached a glass pipette for the micro-iontophoresis of drugs to the juxtacellular recording electrode (**Fig. 4a**). This allowed us to test *in vivo* the local effects of acetylcholine receptor antagonists on the responses of individual VTA neurons to the stimulation of PPN or LDT cholinergic axons. The excitatory responses to the laser in both DA (**Fig. 4b**) and non-DA neurons following the stimulation of either PPN or LDT cholinergic axons were abolished during the iontophoretic administration of nicotinic and muscarinic antagonists in the vicinity (~100 μm above) of the recorded neurons (**Fig. 4c–e**), and were quickly reversed within a few minutes of stopping the micro-iontophoretic current for drug delivery. To further identify the acetylcholine receptors involved, we also performed *ex vivo* whole-cell recordings of VTA neurons and measured their response to local application of the cholinergic agonist carbachol. We observed excitatory responses in DA neurons that were eliminated following the administration of mecamylamine ($t = 7.281$, two-tailed t test, $P = 0.000342$, $n = 9$ neurons), but not methyllycaconitine or DHβE, suggesting a mechanism mediated by nicotinic type-III receptors and independent of GABAergic and glutamatergic transmission (**Supplementary Fig. 8**). These results indicate that the effects on VTA neurons following stimulation of cholinergic axons are a consequence of the release of acetylcholine and not of the release of glutamate or GABA. The specificity of the viral expression for cholinergic neurons is further supported by the absence of glutamate vesicular transporter-2 in PPN and LDT axons expressing the fluorescent reporter in the VTA (**Supplementary Fig. 9**). Thus, in contrast with the short-latency excitatory (presumably glutamatergic)

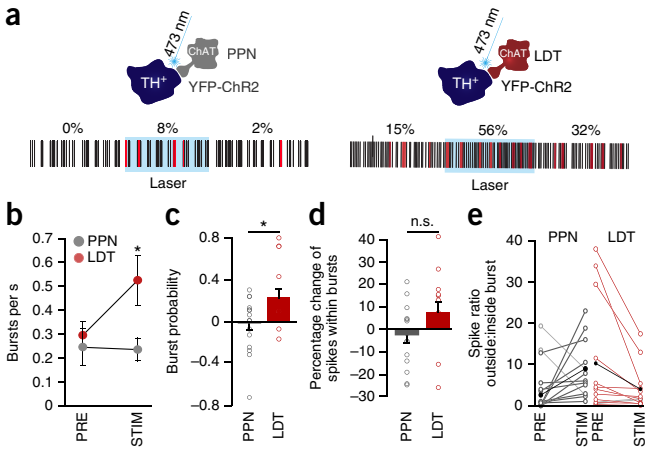

Figure 5 Laser stimulation of cholinergic axons modifies the bursting activity of DA neurons. (**a**) DA neurons modified their bursting activity following optogenetic activation of PPN or LDT cholinergic axons ($n = 15$ of 34 neurons in PPN experiments, $n = 13$ of 26 neurons in LDT experiments). Numbers represent the percentage of spikes in a burst before, during and after laser stimulation. Whereas PPN stimulation tended to switch the pattern of activity of DA neurons, LDT axon stimulation did not change the bursting regime, but did increase the number of spikes in bursts (red) of already bursting neurons. (**b**) LDT axon stimulation significantly increased the number of bursts in those neurons already bursting when compared with the baseline ($F_{1,12} = 7.18$, $P = 0.02$, one-way ANOVA with repeated measures, $n = 13$ neurons in 19 rats) and with PPN axon stimulation ($U = 47.5$, $P = 0.02$, Mann-Whitney, $n = 15$ neurons in 22 rats). (**c**) Increased burst probability during LDT-axon stimulation ($t = 2.18$, two-tailed t test, $P = 0.039$). (**d**) LDT axon stimulation produced more spikes in bursts during the stimulation compared with its baseline ($t = 1.96$, two-tailed t test, $P = 0.06$); when compared with LDT, PPN stimulation resulted in fewer spikes in bursts ($t = 1.76$; two-tailed t test, $P = 0.09$). (**e**) Ratio of spikes outside and inside of bursts during baseline and laser stimulation. During PPN axon stimulation, in all but two cases (light gray), there was a disruption in the bursting activity that was characterized by a larger number of spikes outside of bursts. In contrast, during LDT axon stimulation, in all but two cases (gray) there was an increase in the concentration of spikes in bursts. This change in the ratio was significantly different between PPN ($n = 15$ neurons in 22 rats) and LDT ($n = 13$ neurons in 19 rats; $t = 2.72$; two-tailed t test, $P = 0.011$). Group means are depicted in black. Circles in **b** and bars in **c** and **d** represent average ± s.e.m; asterisks denote significant differences ($P < 0.05$); n.s., not significant.

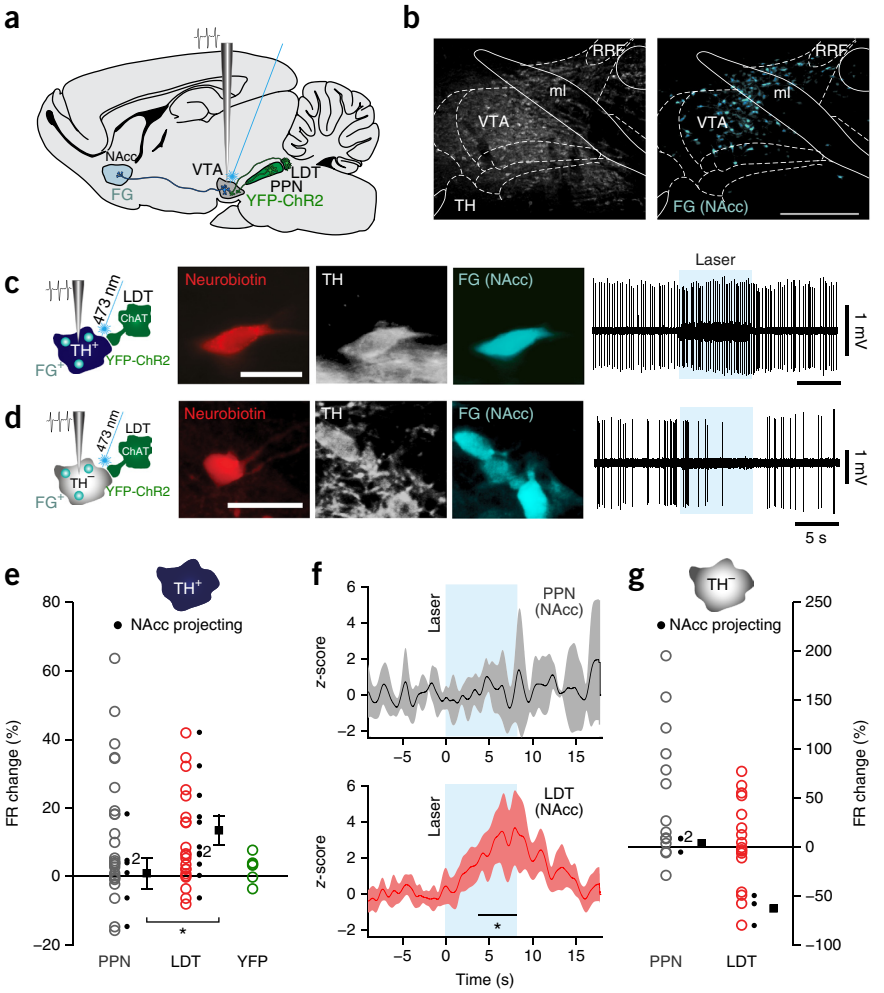

Figure 6 LDT cholinergic axons preferentially target mesolimbic DA and non-DA VTA neurons. (**a**) Schematic of the experimental design. Fluorogold (FG) was injected into the NAcc of ChAT::Cre$^+$ rats that also received a virus injection into the PPN or LDT. (**b**) FG-labeled neurons were observed throughout the VTA, most prominently in the dorsal regions ($n = 27$ rats). (**c**) Example of a FG$^+$ TH$^+$ neuron that was excited by LDT-axon stimulation ($n = 9$ of 11 neurons). (**d**) Example of a FG$^+$ TH$^-$ neuron that was inhibited by LDT axon stimulation ($n = 3$ of 3). The basal firing rate and action potential duration of mesolimbic neurons was not significantly different to that of neurons that did not contain the tracer (TH$^+$, $n = 43$ neurons; TH$^-$, $n = 30$ neurons from 41 rats; basal firing rate: TH$^+$, $U = 322$, $P = 0.854$; TH$^-$, $U = 138$, $P = 0.495$; action potential duration: TH$^+$, $U = 397.5$, $P = 0.649$; TH$^-$, $U = 165.5$, $P = 0.171$, Mann-Whitney). (**e**) DA neurons that projected to the NAcc were preferentially excited by the optogenetic stimulation of LDT cholinergic axons ($n = 11$ neurons in 19 rats). In contrast, PPN-axon stimulation did not activate NAcc-projecting neurons ($n = 6$ neurons in 22 rats; $t = -1.84$, one-tailed t test, $P = 0.04$ between PPN and LDT for NAcc-projecting neurons). Control experiments, in which animals were transduced with YFP alone (no ChR2, green, $n = 5$ rats), did not show a response to the laser. (**f**) Normalized firing rate (mean ± CI) of all TH$^+$ NAcc-projecting neurons following PPN or LDT cholinergic axon stimulation. Black line in the bottom panel represents the time points during which response to LDT stimulation was significantly greater than PPN (cluster-based permutation test, $P = 0.02$, 200 permutations). (**g**) Non-DA neurons that projected to the NAcc were inhibited by LDT axon stimulation, but not by PPN axon stimulation. Black boxes represent means ± s.e.m. of NAcc-projecting neurons in **e** and means in **g**; asterisks denote significant differences ($P < 0.05$). Scale bars represent 500 µm (**b**) and 30 µm (**c**,**d**).

© 2016 Nature America, Inc. All rights reserved.

effects of the electrical stimulation, our findings demonstrate a slow cholinergic modulation of VTA DA neurons arising from both PPN and LDT.

Bursting activity is enhanced by LDT stimulation

In anesthetized rats, DA neurons fire in regular, irregular or bursting mode. We analyzed the spike trains of DA neurons that showed bursting activity during the baseline and/or during optogenetic stimulation of PPN and LDT cholinergic axons. We detected a switch from non-bursting to bursting mode and vice versa only after PPN stimulation. Thus, 27% of neurons that showed bursting activity during the stimulation did not show any bursts during the baseline (**Fig. 5a**). On the other hand, 18% of neurons that were spontaneously bursting during the baseline stopped bursting during the stimulation. This contrasts with LDT axon stimulation that did not elicit any switch to or from bursting activity. Nevertheless, following LDT axon stimulation, neurons that were already firing in bursts during baseline increased their bursting activity (**Fig. 5a**), detected as an increase in the number of bursts episodes (**Fig. 5b**) and a higher burst probability (**Fig. 5c**). Accordingly, we observed a tendency for an increase in the proportion of spikes in bursts only after LDT axon stimulation (**Fig. 5d**). In addition, stimulation of LDT axons led to a decrease in the number of inter-burst spikes when compared with PPN stimulation ($U = 41$, Mann-Whitney, $P = 0.027$; PPN, $n = 13$ neurons; LDT, $n = 13$ neurons; only neurons bursting during laser stimulation). Further differences between PPN and LDT effects were observed: although LDT axon stimulation decreased the ratio of spikes outside bursts to spikes inside bursts (decreasing the burst entropy) in the majority of cases, PPN stimulation tended to produce the opposite effect, disrupting the burst organization (**Fig. 5e**). These data suggest that the effect of PPN cholinergic axon activation is heterogeneous, such that it is able to switch the activity of some DA neurons to bursting mode while disrupting the burst organization in DA neurons that were already bursting. On the other hand, LDT cholinergic axon stimulation reorganizes the spiking into bursts. These data indicate that PPN and LDT cholinergic neurons modulate the activity of DA neurons in the VTA by different mechanisms.

Mesolimbic DA neurons are selectively activated by LDT axons

Given that cholinergic neurons of the PPN and LDT are components of functionally distinct forebrain circuits, we asked whether they might innervate functionally distinct subsets of VTA neurons. We injected a tracer into the nucleus accumbens (NAcc) shell to retrogradely label the so-called mesolimbic neurons in the VTA (**Fig. 6a**). These injections led to labeling predominantly in the dorsal half of the VTA (**Fig. 6b**) and included both DA and non-DA neurons.

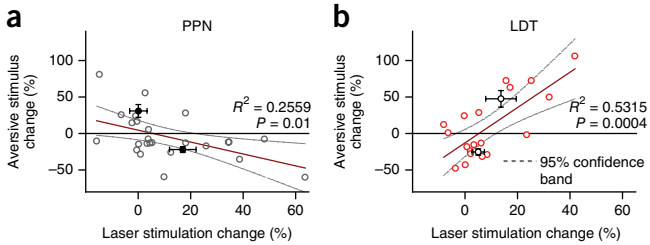

Figure 7 Cholinergic axon stimulation differentially modulates functionally distinct DA neurons. (**a**,**b**) Significant correlations were observed between the change in the firing rate of DA neurons during the hindpaw pinch (aversive stimulus) and their responses to the laser activation of PPN (**a**; $n = 25$ neurons in 22 rats) and LDT (**b**; $n = 19$ neurons in 19 rats) axons. Thus, DA neurons that were more inhibited by the pinch tended to respond more to PPN stimulation (7 of 13) and less to LDT stimulation (3 of 11), whereas DA neurons that were excited by the pinch were more strongly modulated by the LDT (5 of 8) and less by the PPN (1 of 7). Means and s.e.m. for positive or negative values in the change to the aversive stimulus are indicated by black (PPN) and white (LDT) circles with error bars.

We obtained a sample of 17 DA and 6 non-DA neurons that were recorded and labeled using the juxtacellular method and in which the retrograde tracer was also detected (**Fig. 6c**,**d**). We observed that mesolimbic DA neurons had a greater excitatory response following LDT axon stimulation than following PPN axon stimulation (**Fig. 6e**,**f**). Those DA neurons that increased their firing rate following PPN axon stimulation lacked the retrograde tracer (**Fig. 6e**), suggesting that they innervate a subset of neurons that project to other VTA targets. In contrast, mesolimbic non-DA neurons were inhibited by LDT, but not PPN, axon stimulation (**Fig. 6g**).

Cholinergic axons differentially modulate DA functional circuits

Midbrain DA neurons have been classically associated with reward mechanisms[1,4]. Although the majority of them increase their firing in response to motivating stimuli and are consequently inhibited by aversive stimuli, a proportion of them are excited by noxious (aversive) stimuli[30,31]. This can be emulated in the anesthetized rat by a hind-paw pinch[32] or foot shock[23]. Such differences in responses have been proposed to be associated with the functional pathways in which DA neurons are integrated[11,22]. From all of the neurons that were activated by the aversive stimulation, we identified nearly half of them as being NAcc projecting (7 of 15 neurons), which contrasts with the lower of number of neurons inhibited by the stimulation that were identified as being NAcc projecting (7 of 26 neurons). We then correlated the responses of DA neurons to the hind-paw pinch with their responses to the optogenetic activation of the cholinergic axons arising in PPN or LDT (**Supplementary Fig. 10**). We observed an opposite trend in the effect of PPN and LDT drive:

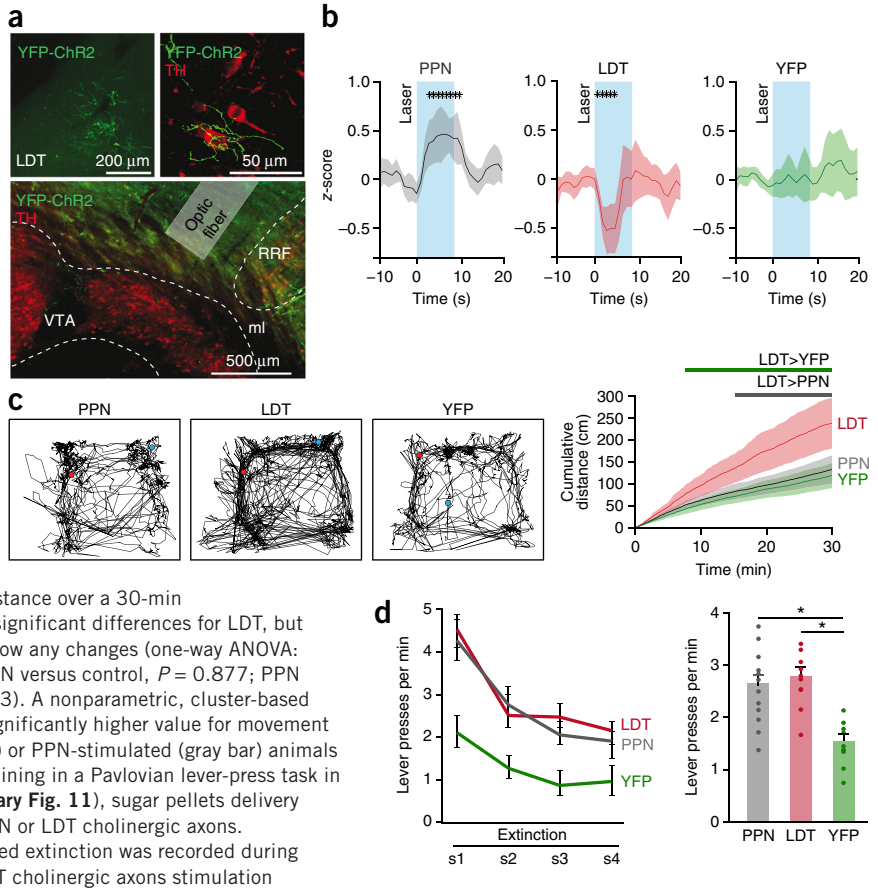

Figure 8 Optogenetic activation of cholinergic axons in the VTA in behaving rats. (**a**) Cholinergic neurons of the PPN and LDT were transduced with YFP and ChR2, and an optic fiber was chronically implanted above the VTA ($n_{PPN} = 12$, $n_{LDT} = 10$, $n_{WT} = 10$ rats). (**b**) Optogenetic activation of cholinergic axons in the VTA produced different effects on stimulation-locked locomotor activity (10 Hz, 50 ms, 80 pulses, 13 stimulations): PPN axon stimulation increased motor activity, whereas LDT axon stimulation decreased it. No changes were observed in control animals (two-way ANOVA; stimulation effect $F_{2,58} = 3.569$, $P = 0.035$; group effect $F_{2,58} = 0.325$, $P = 0.725$; interaction $F_{4,58} = 16.58$, $P = 0.004115$; *post hoc* comparisons PPN versus WT, $P = 0.029$; PPN versus LDT, $P = 0.000028$; LDT versus WT, $P = 0.044$). Asterisks represent significantly different time-points following laser stimulation based on a nonparametric cluster-based comparison ($P = 0.002$, $n = 500$ permutations). (**c**) Representative tracking traces and cumulative distance over a 30-min recording with pulses delivered every 2 min showed significant differences for LDT, but not PPN, axon stimulation; control animals do not show any changes (one-way ANOVA: $F_{2,31} = 9.353$, $P = 0.001$; *post hoc* comparisons: PPN versus control, $P = 0.877$; PPN versus LDT, $P = 0.001$; LDT versus control, $P = 0.003$). A nonparametric, cluster-based two-tailed *t* test analysis revealed that there was a significantly higher value for movement in LDT-stimulated animals than in control (green bar) or PPN-stimulated (gray bar) animals ($P = 0.002$, $n = 500$ permutations). (**d**) Following training in a Pavlovian lever-press task in a progressive random interval schedule (**Supplementary Fig. 11**), sugar pellets delivery was replaced by optogenetic stimulation of either PPN or LDT cholinergic axons. Control animals also received laser pulses. Conditioned extinction was recorded during four consecutive days (s, session; 1–4). PPN and LDT cholinergic axons stimulation produced a slowing in extinction compared with the control group, as shown by a significantly higher number of lever presses in PPN and LDT groups (two-way ANOVA; day effect: $F_{3,27} = 15.747$, $P = 0.000004$; group effect: $F_{2,29} = 13.781$, $P = 0.000062$; interaction: $F_{6,54} = 0.785$, $P = 0.586$; *post hoc* comparisons: PPN versus LDT, $P = 0.839$; PPN versus control, $P = 0.000392$; LDT versus control, $P = 0.000148$). Data in **b** and **c** are depicted as mean ± CI; data in **d** are depicted as mean ± s.e.m. $^*P < 0.05$.

© 2016 Nature America, Inc. All rights reserved.

whereas PPN axon stimulation tended to modulate more consistently those neurons that showed a greater inhibition to the pinch (**Fig. 7a**), LDT axon stimulation more robustly modulated the neurons that were excited by the pinch (**Fig. 7b**). Indeed, 75% (6 of 8) of aversive stimuli-excited DA neurons increased the number of spikes in the bursts during LDT axon stimulation; in contrast, 85% of aversive stimuli-excited DA neurons (6 of 7) decreased their number of spikes in bursts or switched to non-bursting mode during PPN axon stimulation. Although the numbers of neurons are low, and the conclusions should be taken with caution, these results further support the notion that subsets of DA neurons that receive cholinergic afferents from the PPN and LDT are organized into functionally distinct pathways arising in the VTA.

Cholinergic neurons convey reinforcing signals, but dissociate locomotor effects

Neurons of the PPN and LDT have been proposed to facilitate reward-related behavior through the modulation of midbrain DA neurons[33–35]. In addition, activation of DA neurons elicits locomotion that is presumably mediated by DA release in striatal circuits[36]. We tested the consequences of differentially activating cholinergic axons in freely moving rats with chronically implanted optic fibers above the VTA in an open field and during an instrumental lever-pressing task (**Fig. 8a**). Optogenetic activation of PPN and LDT cholinergic axons in an open field produced contrasting effects: PPN transiently increased motor activity, whereas LDT decreased locomotion (**Fig. 8b**). However, the overall effect from LDT stimulation facilitated movement, reflected by the increased cumulative distance over the full testing session. PPN stimulation did not produce a cumulative effect on locomotion (**Fig. 8c**). All of the locomotor effects elicited by optogenetic stimulation were abolished by the systemic administration of acetylcholine receptor antagonists (as used above; **Supplementary Fig. 11**). Separately, rats were trained to lever press to obtain sugar pellets. Following the acquisition, sugar pellets were replaced by optogenetic stimulation of cholinergic axons during lever presses. Activation of either PPN or LDT cholinergic axons was sufficient to significantly slow-down lever-press extinction compared with wild-type rats (**Fig. 8d**). Notably, *post hoc* analysis revealed that PPN and LDT groups were not different from each other. These results suggest that, although both PPN and LDT cholinergic neurons produce similar effects during reinforcement, they induce distinct motor effects that may reflect the differential output of DA neurons.

DISCUSSION

We found that two brainstem cholinergic nuclei, one typically associated with motor and arousal functions and the other with reward, have differential effects on subsets of neurons in VTA. First, we observed that cholinergic neurons of the PPN and LDT projected extensively throughout most of VTA. Second, stimulation of either of the two cholinergic pathways produced a slow modulation of the firing rate of DA and non-DA neurons; effects that were mediated by acetylcholine. Third, cholinergic modulation of DA neurons took on two different forms depending on the source of innervation: PPN axon stimulation switched the firing pattern to bursting mode in a proportion of DA neurons and increased the level of entropy in the spike train of most neurons, whereas LDT axon stimulation enhanced the organization in bursting spike trains. Fourth, LDT axons predominantly targeted mesolimbic DA neurons that were excited by aversive stimulation, whereas PPN axons targeted a distinct subset of DA neurons that were predominantly inhibited by aversive stimulation. Fifth, PPN axons transiently induced motor activity, whereas LDT axons had the opposite effect. Our findings therefore suggest that functional segregation of brainstem cholinergic neurons is maintained at the level of the VTA and is underpinned by differential modulation of subpopulations of DA and non-DA neurons.

Functional microcircuits in the VTA

DA neurons receive excitatory afferents from several regions of the brain, including the prefrontal cortex, the lateral hypothalamic and lateral preoptic area, and the brainstem[6,25]. The projections originating in the PPN and LDT are heterogeneous and consist of cholinergic, glutamatergic and GABAergic components[37–39]. Although PPN and LDT are structurally and neurochemically similar[40], and indeed share some of their afferent and efferent connections[41], they differ in the functional circuits to which they contribute. For example, the PPN is connected to structures involved in motor (including most regions of the basal ganglia[42]) and arousal functions[19]. On the other hand, LDT is connected to cortical and thalamic regions associated with the limbic system[18,20,43]. The VTA, in turn, is heterogeneous, with distinct distributions of DA neurons that project to different targets involved in different functional pathways[11,25]. We hypothesized that the two cholinergic pathways have different effects in the VTA and possibly differentially target subpopulations of DA neurons. Our anatomical data revealed that the projections from both PPN and LDT innervated most of the VTA and, indeed, DA and non-DA neurons that were modulated by PPN axons were intermingled in the same VTA regions as those modulated by LDT axons. Nevertheless, LDT cholinergic axons selectively targeted mesolimbic DA neurons, whereas PPN axons had little influence on them. In contrast, PPN axons primarily modulated DA neurons that were components of different circuits and whose targets have not yet been determined (for example, amygdala and hippocampus). This suggests that neighboring DA neurons can be differentially modulated by cholinergic afferents that encode either motor or limbic signals. The motor-limbic segregation is maintained in other brainstem cholinergic targets, most notably the striatum: cholinergic LDT neurons that innervate the NAcc send collaterals that innervate the midline thalamus and the VTA, both of which in turn also project to the NAcc[44]. This suggests that the cholinergic LDT neurons that modulate mesolimbic DA neurons also target postsynaptic structures in the NAcc, and potentially converge with the axons of the same mesolimbic DA neurons that they modulate in the VTA.

We also observed that cholinergic LDT axons showed a higher degree of collateralization in the VTA and contacted a higher proportion of non-DA neurons than PPN cholinergic axons. Thus, LDT cholinergic neurons may have a greater influence on non-DA neurons than PPN cholinergic neurons. This suggestion may be consistent with some of our observations in the LDT optogenetics experiments. First, the late-responding DA neurons (**Fig. 2h**) may represent a rebound excitation following the excitation of GABAergic interneurons. Second, mesolimbic non-DA neurons (putative GABAergic) that were inhibited by cholinergic activation (**Fig. 6d**) may act in coordination with DA neurons to reinforce DA transmission in the NAcc (for example, by inhibiting cholinergic neurons in NAcc[45]). Overall, our data suggest multiple functional mechanisms by which the cholinergic brainstem neurons may influence the activity of limbic circuits.

Cholinergic brainstem neurons in salience and reward

Cholinergic neurons of the brainstem have been conceptually associated with the reticular activating system. Sensory stimulation triggers a phasic activation of PPN cholinergic neurons[46] that, in turn, increase the responsiveness of their target neurons, enabling them to

© 2016 Nature America, Inc. All rights reserved.

bind other modalities of stimuli[47]. This suggests a role in salience, where cholinergic neurons signal the presence of potentially relevant cues that, in turn, increase the level of behavioral arousal[48]. Recent evidence, however, points to a more specific role of the PPN in coding reward and reward-prediction error[34,35], suggesting that PPN neurons also encode motivational value. Our data support the notion that both PPN and LDT provide a reinforcing signal to DA neurons. Nevertheless, cholinergic neurons only constitute a fraction of the PPN and LDT; indeed, glutamatergic neurons may also modulate the activity of DA neurons, either directly or indirectly through cholinergic neurons[49]. Glutamatergic neurons, however, have different connectivity and dynamic properties as cholinergic neurons[46,50], suggesting that they are likely to have different, if not complementary, effects on VTA neurons.

Our findings also indicate that activation of brainstem cholinergic axons changes the bursting behavior of DA neurons. Activation of PPN axons produced bursting in some neurons while increasing the ratio of spikes outside of bursts in the majority of responding DA neurons. In contrast, LDT afferents reorganized the spike train into bursts. These differences may give clues to the specific functions of these cholinergic neurons. By switching the discharge mode of DA neurons, PPN afferents may be triggering a state change in which neurons disengage from their preceding activity and increase their responsiveness to other inputs, consistent with the notion of both, an arousal system that generates orienting or attentional responses, and a motor system that facilitates motor output, as observed in our experiments. In contrast, by increasing the number of spikes in bursts, the LDT increases the amount of information contained in each burst, equivalent to increasing the value associated with a reward prediction. Stimulation of LDT axons produced an overall kinetic effect that is likely the result of inducing DA release from mesolimbic neurons[36], triggered by a slow dynamics that resemble the time course in the response of DA neurons (**Fig. 2h**). Notably, we detected a fast and transient inhibitory effect on motor activity that may be associated with a shorter latency in the response of non-DA neurons to cholinergic activation; an observation that deserves further investigation. Thus, the differences that we observed may underlie the neuronal basis of saliency and reward at the level of the cholinergic brainstem and VTA neurons (also see ref. 35).

In summary, cholinergic neurons of the brainstem provide a functionally segregated modulation of DA and non-DA neurons of the VTA, consistent with their connectivity with other structures in motor and limbic circuits in the basal ganglia and thalamus. Our findings therefore demonstrate the importance of the cholinergic inputs for the modulation of DA neuron function. It remains to be established how brainstem cholinergic neurons work in concert with brainstem glutamatergic neurons at the level of both the midbrain and the striatum to shape behavior and to determine an organism's response to reward-related stimuli.

METHODS

Methods and any associated references are available in the online version of the paper.

Note: Any Supplementary Information and Source Data files are available in the online version of the paper.

ACKNOWLEDGMENTS

We thank M. Ungless for discussions on a previous version of this manuscript, A. Asif-Malik for training rats in the operant task, and E. Norman, L. Conyers and L. Black for their technical assistance. This work was supported by the Medical Research Council UK and by a Leverhulme Trust grant to J.M.-S. and T.V.G. (RPG-2012-690). D.D. was funded by a University of Leicester PhD studentship. A.S.S. was supported by People Marie Curie Actions: Latin America and Europe Liaison and Universidade Federal de Mato Grosso do Sul.

AUTHOR CONTRIBUTIONS

J.M.-S. conceived and supervised the project. D.D. and A.S.S. performed *in vivo* experiments and anatomical tracing. I.H.-O. performed the electron microscopy and analyzed the data. M.A. performed the *in vitro* experiments under the supervision of J.M.T. D.D. performed the behavioral experiments under the supervision of T.V.G. M.V., D.D., J.P.B., I.H.-O., T.V.G. and J.M.-S. analyzed the data. I.B.W. and K.D. provided the transgenic rats. D.D., J.P.B. and J.M.-S. wrote the manuscript.

COMPETING FINANCIAL INTERESTS

The authors declare no competing financial interests.

Reprints and permissions information is available online at http://www.nature.com/reprints/index.html.

1. Wise, R.A. Dopamine, learning and motivation. *Nat. Rev. Neurosci.* **5**, 483–494 (2004).
2. Montague, P.R., Hyman, S.E. & Cohen, J.D. Computational roles for dopamine in behavioural control. *Nature* **431**, 760–767 (2004).
3. Joshua, M. *et al.* Synchronization of midbrain dopaminergic neurons is enhanced by rewarding events. *Neuron* **62**, 695–704 (2009).
4. Schultz, W. Updating dopamine reward signals. *Curr. Opin. Neurobiol.* **23**, 229–238 (2013).
5. Tsai, H.C. *et al.* Phasic firing in dopaminergic neurons is sufficient for behavioral conditioning. *Science* **324**, 1080–1084 (2009).
6. Sesack, S.R. & Grace, A.A. Cortico-Basal Ganglia reward network: microcircuitry. *Neuropsychopharmacology* **35**, 27–47 (2010).
7. Mena-Segovia, J., Winn, P. & Bolam, J.P. Cholinergic modulation of midbrain dopaminergic systems. *Brain Res. Rev.* **58**, 265–271 (2008).
8. Floresco, S.B., West, A.R., Ash, B., Moore, H. & Grace, A.A. Afferent modulation of dopamine neuron firing differentially regulates tonic and phasic dopamine transmission. *Nat. Neurosci.* **6**, 968–973 (2003).
9. Lokwan, S.J., Overton, P.G., Berry, M.S. & Clark, D. Stimulation of the pedunculopontine tegmental nucleus in the rat produces burst firing in A9 dopaminergic neurons. *Neuroscience* **92**, 245–254 (1999).
10. Lodge, D.J. & Grace, A.A. The laterodorsal tegmentum is essential for burst firing of ventral tegmental area dopamine neurons. *Proc. Natl. Acad. Sci. USA* **103**, 5167–5172 (2006).
11. Lammel, S. *et al.* Input-specific control of reward and aversion in the ventral tegmental area. *Nature* **491**, 212–217 (2012).
12. Clarke, P.B. & Pert, A. Autoradiographic evidence for nicotine receptors on nigrostriatal and mesolimbic dopaminergic neurons. *Brain Res.* **348**, 355–358 (1985).
13. Calabresi, P., Lacey, M.G. & North, R.A. Nicotinic excitation of rat ventral tegmental neurones in vitro studied by intracellular recording. *Br. J. Pharmacol.* **98**, 135–140 (1989).
14. Lacey, M.G., Calabresi, P. & North, R.A. Muscarine depolarizes rat substantia nigra zona compacta and ventral tegmental neurons in vitro through M1-like receptors. *J. Pharmacol. Exp. Ther.* **253**, 395–400 (1990).
15. Zhang, L., Liu, Y. & Chen, X. Carbachol induces burst firing of dopamine cells in the ventral tegmental area by promoting calcium entry through L-type channels in the rat. *J. Physiol. (Lond.)* **568**, 469–481 (2005).
16. Yeomans, J. & Baptista, M. Both nicotinic and muscarinic receptors in ventral tegmental area contribute to brain-stimulation reward. *Pharmacol. Biochem. Behav.* **57**, 915–921 (1997).
17. Miller, A.D. & Blaha, C.D. Midbrain muscarinic receptor mechanisms underlying regulation of mesoaccumbens and nigrostriatal dopaminergic transmission in the rat. *Eur. J. Neurosci.* **21**, 1837–1846 (2005).
18. Semba, K. & Fibiger, H.C. Afferent connections of the laterodorsal and the pedunculopontine tegmental nuclei in the rat: a retro- and antero-grade transport and immunohistochemical study. *J. Comp. Neurol.* **323**, 387–410 (1992).
19. Steriade, M. Arousal: revisiting the reticular activating system. *Science* **272**, 225–226 (1996).
20. Cornwall, J., Cooper, J.D. & Phillipson, O.T. Afferent and efferent connections of the laterodorsal tegmental nucleus in the rat. *Brain Res. Bull.* **25**, 271–284 (1990).
21. Lammel, S. *et al.* Unique properties of mesoprefrontal neurons within a dual mesocorticolimbic dopamine system. *Neuron* **57**, 760–773 (2008).
22. Matsumoto, M. & Hikosaka, O. Two types of dopamine neuron distinctly convey positive and negative motivational signals. *Nature* **459**, 837–841 (2009).
23. Brischoux, F., Chakraborty, S., Brierley, D.I. & Ungless, M.A. Phasic excitation of dopamine neurons in ventral VTA by noxious stimuli. *Proc. Natl. Acad. Sci. USA* **106**, 4894–4899 (2009).
24. Roeper, J. Dissecting the diversity of midbrain dopamine neurons. *Trends Neurosci.* **36**, 336–342 (2013).

© 2016 Nature America, Inc. All rights reserved.

25. Ikemoto, S. Dopamine reward circuitry: two projection systems from the ventral midbrain to the nucleus accumbens-olfactory tubercle complex. *Brain Res. Rev.* **56**, 27–78 (2007).
26. Bromberg-Martin, E.S., Matsumoto, M. & Hikosaka, O. Dopamine in motivational control: rewarding, aversive, and alerting. *Neuron* **68**, 815–834 (2010).
27. Witten, I.B. *et al.* Recombinase-driver rat lines: tools, techniques, and optogenetic application to dopamine-mediated reinforcement. *Neuron* **72**, 721–733 (2011).
28. Scarnati, E., Proia, A., Campana, E. & Pacitti, C. A microiontophoretic study on the nature of the putative synaptic neurotransmitter involved in the pedunculopontine-substantia nigra pars compacta excitatory pathway of the rat. *Exp. Brain Res.* **62**, 470–478 (1986).
29. Futami, T., Takakusaki, K. & Kitai, S.T. Glutamatergic and cholinergic inputs from the pedunculopontine tegmental nucleus to dopamine neurons in the substantia nigra pars compacta. *Neurosci. Res.* **21**, 331–342 (1995).
30. Mantz, J., Thierry, A.M. & Glowinski, J. Effect of noxious tail pinch on the discharge rate of mesocortical and mesolimbic dopamine neurons: selective activation of the mesocortical system. *Brain Res.* **476**, 377–381 (1989).
31. Coizet, V., Dommett, E.J., Redgrave, P. & Overton, P.G. Nociceptive responses of midbrain dopaminergic neurones are modulated by the superior colliculus in the rat. *Neuroscience* **139**, 1479–1493 (2006).
32. Ungless, M.A., Magill, P.J. & Bolam, J.P. Uniform inhibition of dopamine neurons in the ventral tegmental area by aversive stimuli. *Science* **303**, 2040–2042 (2004).
33. Dormont, J.F., Condé, H. & Farin, D. The role of the pedunculopontine tegmental nucleus in relation to conditioned motor performance in the cat. I. Context-dependent and reinforcement-related single unit activity. *Exp. Brain Res.* **121**, 401–410 (1998).
34. Okada, K., Toyama, K., Inoue, Y., Isa, T. & Kobayashi, Y. Different pedunculopontine tegmental neurons signal predicted and actual task rewards. *J. Neurosci.* **29**, 4858–4870 (2009).
35. Hong, S. & Hikosaka, O. Pedunculopontine tegmental nucleus neurons provide reward, sensorimotor, and alerting signals to midbrain dopamine neurons. *Neuroscience* **282C**, 139–155 (2014).
36. Johnson, K., Churchill, L., Klitenick, M.A., Hooks, M.S. & Kalivas, P.W. Involvement of the ventral tegmental area in locomotion elicited from the nucleus accumbens or ventral pallidum. *J. Pharmacol. Exp. Ther.* **277**, 1122–1131 (1996).
37. Bevan, M.D. & Bolam, J.P. Cholinergic, GABAergic, and glutamate-enriched inputs from the mesopontine tegmentum to the subthalamic nucleus in the rat. *J. Neurosci.* **15**, 7105–7120 (1995).
38. Charara, A., Smith, Y. & Parent, A. Glutamatergic inputs from the pedunculopontine nucleus to midbrain dopaminergic neurons in primates: Phaseolus vulgaris-leucoagglutinin anterograde labeling combined with postembedding glutamate and GABA immunohistochemistry. *J. Comp. Neurol.* **364**, 254–266 (1996).
39. Omelchenko, N. & Sesack, S.R. Laterodorsal tegmental projections to identified cell populations in the rat ventral tegmental area. *J. Comp. Neurol.* **483**, 217–235 (2005).
40. Wang, H.L. & Morales, M. Pedunculopontine and laterodorsal tegmental nuclei contain distinct populations of cholinergic, glutamatergic and GABAergic neurons in the rat. *Eur. J. Neurosci.* **29**, 340–358 (2009).
41. Woolf, N.J. & Butcher, L.L. Cholinergic systems in the rat brain: III. Projections from the pontomesencephalic tegmentum to the thalamus, tectum, basal ganglia, and basal forebrain. *Brain Res. Bull.* **16**, 603–637 (1986).
42. Mena-Segovia, J., Bolam, J.P. & Magill, P.J. Pedunculopontine nucleus and basal ganglia: distant relatives or part of the same family? *Trends Neurosci.* **27**, 585–588 (2004).
43. Bolton, R.F., Cornwall, J. & Phillipson, O.T. Collateral axons of cholinergic pontine neurones projecting to midline, mediodorsal and parafascicular thalamic nuclei in the rat. *J. Chem. Neuroanat.* **6**, 101–114 (1993).
44. Dautan, D. *et al.* A major external source of cholinergic innervation of the striatum and nucleus accumbens originates in the brainstem. *J. Neurosci.* **34**, 4509–4518 (2014).
45. Brown, M.T. *et al.* Ventral tegmental area GABA projections pause accumbal cholinergic interneurons to enhance associative learning. *Nature* **492**, 452–456 (2012).
46. Petzold, A., Valencia, M., Pál, B. & Mena-Segovia, J. Decoding brain state transitions in the pedunculopontine nucleus: cooperative phasic and tonic mechanisms. *Front. Neural Circuits* **9**, 68 (2015).
47. Munk, M.H., Roelfsema, P.R., König, P., Engel, A.K. & Singer, W. Role of reticular activation in the modulation of intracortical synchronization. *Science* **272**, 271–274 (1996).
48. Pan, W.X. & Hyland, B.I. Pedunculopontine tegmental nucleus controls conditioned responses of midbrain dopamine neurons in behaving rats. *J. Neurosci.* **25**, 4725–4732 (2005).
49. Good, C.H. & Lupica, C.R. Properties of distinct ventral tegmental area synapses activated via pedunculopontine or ventral tegmental area stimulation in vitro. *J. Physiol. (Lond.)* **587**, 1233–1247 (2009).
50. Boucetta, S., Cissé, Y., Mainville, L., Morales, M. & Jones, B.E. Discharge profiles across the sleep-waking cycle of identified cholinergic, GABAergic, and glutamatergic neurons in the pontomesencephalic tegmentum of the rat. *J. Neurosci.* **34**, 4708–4727 (2014).

© 2016 Nature America, Inc. All rights reserved.

npg

ONLINE METHODS

Animals. Male adult (250–450 g) Long Evans (LE) wild-type and ChAT::Cre$^+$ (ref. 27) rats were used for all experiments. Rats were maintained on a 12-h light cycle (lights on 07:00), were group housed and had *ad libitum* access to water and food. All procedures were performed in accordance with the Society for Neuroscience policy on the use of animals in neuroscience and the Animals (Scientific Procedures) Act, 1986 (UK) and EU Directive 2010/63/EU, under the authority of Project License 30-2639 approved by the Home Office and the local ethical committee of the University of Oxford.

Stereotaxic Injections. All stereotaxic injections were performed during deep isofluorane anesthesia (2–4% in O_2; Isoflo, Schering-Plough). For the anatomical studies, the rats (n = 4, LE wild-type) were injected with Cholera toxin b (CTb, 2.5% in water, 100 nl over 10 min; Sigma-Aldrich, cat. number C9903) in the rostral VTA (from Bregma in mm, AP: −5.2; ML: 0.8; DV: 7.5 ventral of the dura) and red retrobeads (RB-R, 150 nl over 10 min; Lumafluor) in the caudal VTA (from Bregma in mm, AP: −5.8; ML: 1.1; DV: 7.7 ventral of the dura) to retrogradely label PPN and LDT neurons that innervate the VTA. Six ChAT::Cre$^+$ rats were injected with adeno-associated virus serotypes 2 (AAV2) and 5 (AAV5) carrying fusion genes for ChR2 and YFP or mCherry (University of North Carolina Gene Therapy Center Virus Vector Core). Thus, we injected either AAV2-EF1a-DIO-eYFP in the PPN (500 nl over 10 min; from Bregma in mm, AP: −7.8; ML: 1.8; DV: 6.5 ventral of the dura) and AAV5-EF1a-DIO-mCherry in the LDT (300 nl over 10 min; from Bregma in mm, AP: −8.5; ML: 0.9; DV: 6.0 ventral of the dura), or AAV2-EF1a-DIO-eYFP in the LDT (n = 3 rats), to quantify the transduction rate of cholinergic neurons (YFP in PPN and mCherry in LDT) and anterogradely label the cholinergic axons innervating the VTA (YFP in LDT). Additional injections (500 nl over 10 min) were delivered in other brain areas to evaluate non-specific expression of the virus (all coordinates from Bregma in mm): cerebellum (AP: −10.0; ML: 1.5; DV: −5.5), superior colliculus (AP: −6.4; ML: 1.0; DV: −4.0), dorsal striatum (AP: +1.5; ML: 2.5; DV: −5.0) and thalamus (AP: −4.0; ML: 2.2; DV: −4.5). The PPN injections led to a roughly spherical transduction of about 1-mm diameter, and LDT injections about 0.5 mm. In each experiment, the transduced area was verified to be largely restricted to the PPN or LDT by analyzing under a fluorescence microscope the rostro-caudal distribution of YFP-expressing neurons.

For the rats used for the electrophysiological studies, we first injected AAV2-EF1a-DIO-hChR2-eYFP into the PPN or LDT of ChAT::Cre$^+$ rats to transduce cholinergic neurons, as described above (n = 41 rats). 2 weeks later, we injected Fluorogold (FG; 2.0%, 300 nl over 10 min; Fluorochrome, LLC) or CTb (2.5%, 500 nl over 10 min; Sigma-Aldrich) in the lateral shell of the NAcc (from Bregma in mm, AP: +1.2; ML: 2.7; DV: 6.8 ventral of the dura); the tracers were alternated between animals. For the pharmacology experiments, only AAV2-EF1a-DIO-hChR2-YFP was injected into the PPN or LDT (n = 9 rats). For control experiments, AAV5-EF1a-DIO-mCherry or AAV2-EF1a-DIO-eYFP (that is, without ChR2; n = 6 rats) were injected in PPN and LDT in ChAT::Cre$^+$ rats as described above. All injections were made using designated 1-µl syringes (SGE Analytical Science) for each vector at a rate of 50 nl/min and a post-injection diffusion time of 5 min. 10–15 d later, juxtacellular recordings and labeling of neurons were performed in the VTA.

Juxtacellular recording. Anesthesia was induced with 4% isofluorane (vol/vol, Schering-Plough) in O_2, and maintained by an injection of urethane (1.3 g per kg of body weight, intraperitoneal (i.p.); ethyl carbamate; Sigma). Supplemental doses of ketamine (35 mg/kg, i.p.; Ketaset, Willows Francis) and xylazine (6 mg/kg, i.p.; Rompun) were administered as required throughout the experiment. Body temperature was maintained at 38 °C using a thermistor-controlled heating pad. After local skin anesthesia by a subcutaneous injection of bupivacaine (0.25%, wt/vol; Astra), the animals were placed in a stereotaxic frame (Kopf). A cutaneous incision was made to expose the skull. Then, craniotomies were made for the electrocorticogram (ECoG; bilaterally, from bregma, AP: +3.0 mm; ML: ±2.5 mm; corresponding to the somatic sensorimotor cortex) and its reference (above the right cerebellum), and the optic fiber cannula (from Bregma in mm, AP: +8.8; ML: 0.8: DV: 6.2 ventral of the dura, implanted at a 20° angle; aimed at the site where cholinergic axon bundles that originate in the brainstem penetrate the caudal VTA, as identified in our anatomical studies). A small craniotomy was made above the VTA (from Bregma in mm, AP: −4.0 to −5.3; ML: 0.4 to 1.4, to be used at a 5° angle) and the dura mater was gently removed to allow the passage of a glass pipette for single cell recordings; the exposed brain surface was kept moist with sterile saline (0.9% NaCl) throughout the experiment. A supplementary ground for the single cell electrode was placed subcutaneously at the back of the neck.

The ECoG was recorded using 1-mm diameter stainless steel screws and referenced to a steel screw above the cerebellum. ECoG signals were band-pass filtered at 0.3–1,000 Hz (−3-dB limits), amplified 2,000–fold (DPA-2FS filter/amplifier; Scientifica) and digitized online at 2.5 kHz. The ECoG was used to monitor the depth of anesthesia. The anesthetics used typically produce slow-wave activity alternating with episodes of spontaneous cortical activation[51]. Extracellular recordings of action potentials of individual VTA neurons were made using glass micropipettes (15–25 MΩ, measured in the cortex; tip diameter ~1.5 µm) filled with 1.5% neurobiotin (wt/vol, Vector Laboratories) in 0.5 M NaCl. Signals from the glass micropipettes were band-pass filtered at 0.3–5,000 Hz (NL125: Digitimer), amplified tenfold through the active bridge circuitry of an Axoprobe-1A amplifier (Molecular Devices), AC-coupled and amplified a further 100-fold (NL-106 AC-DC Amp. Digitimer), and digitized online at 17.5 kHz. Data were acquired and stored using an analog-to-digital converter (Power 1401; Cambridge Electronic Design) connected to a PC running Spike2 (ver. 7; Cambridge Electronic Design).

A multimode fiber optic patch cable (300-µm diameter, 2 m long; M56L01, ThorLabs) was lowered to the VTA and connected to one end of the implanted ceramic cannula (300-µm diameter, 10 mm long; CFMC13L10, ThorLabs) using a mating sleeve, and the other end was connected to a class IIIb blue laser (473 nm; LRS-0473-PFM-00100-05, LaserGlow Technologies). At the beginning of each experiment, the output power of the laser at the cannula end was measured and adjusted to deliver ~20 mW. The laser in turn was driven by transistor-transistor logic (TTL) pulses originating in the digital output of the Power 1401 (Cambridge Electronic Design) and fed back to its digital input to record the stimulation events. The stimulation protocol was set as follows: pulse duration 50 ms and frequency of 10 Hz. Train pulses were repeated twice at least, with a minimum interval of 30 s between each.

All regions of the VTA were scanned with the glass micropipettes for spontaneously firing neurons. When action potentials were detected, a minimum of 5 min of activity was recorded to establish a mean baseline firing rate and spontaneous discharge pattern. Subsequently, sensory stimulation was elicited by a pinch of the hind paw delivering a standard pressure of 183 g/mm^2 (aversive stimulus). Once the firing rate returned to the baseline (approximately 5 min), the activity of putative VTA neurons was recorded during optical stimulation of brainstem cholinergic afferents. At the end of the recording, a micro-iontophoretic current was applied to the neuron (1–10-nA positive current, 200-ms duration, 50% duty cycle) to label it with the neurobiotin[52]. To achieve reliable labeling, the firing of the neuron had to be robustly modulated by the current injection for a minimum of 1 min. The neurobiotin was allowed to transport along the neuronal processes for 2–4 h. To ensure discrimination between neurons during the histological analysis (see below), a maximum of four neurons were labeled per animal with a minimum distance from each other of 400 µm in all axes. Following the diffusion time, the animals were given a lethal dose of ketamine (150 mg/kg) and transcardially perfused with 0.05 M phosphate buffered saline (PBS), pH 7.4, followed by 300 ml of 4% paraformaldehyde (wt/vol) in phosphate buffer (0.1 M, pH 7.4). Brains were stored in PBS at 4 °C until sectioning.

Micro-iontophoresis. An *in vivo* iontophoretic drug delivery procedure was adapted from previous reports[53,54] to allow recording, laser stimulation, drug delivery and labeling of individual VTA neurons. Custom-made double-barrel pipettes were prepared by combining a single glass capillary for juxtacellular recording/labeling (2-µm tip diameter, resistance 15–20 MΩ) and an additional glass capillary at an angle of ~20° for drug infusion (10-µm tip diameter) connected to a iontophoresis pump system (Neurophore BH-2, Digitimer). Both pipettes tips were glued with cyanoacrylate first, situating the tip of the iontophoresis capillary at an average distance of 100 µm above the tip of the juxtacellular capillary, and reinforced using epoxy and dental cement. During the experiments, a baseline recording was obtained, during which VTA neurons were stimulated with the laser using the parameters described above (80 pulses, 10 Hz, 50-ms duration). Following a recovery period, a cocktail of nicotinic and muscarinic antagonists was applied by iontophoresis (80 nA, 50-ms injection, 1 Hz),

© 2016 Nature America, Inc. All rights reserved.
npg

doi:10.1038/nn.4335

consisting of the following: methyllycaconitine (MLA) 20 mM, dihydro-β-erythroidine (DHβE) 40 mM, atropine 40 mM and mecamylamine 100 μM. All drugs were dissolved in 0.9% saline solution. The injection was controlled by adjusting the current and the resistance of the drug injection pipettes. Current injection was counterbalanced using the recording electrode. Neurons were stimulated again with the laser during the drug administration. A minimum of three laser trials were delivered with a minimum of 60 s between each. After 300 s of drug iontophoresis, the injection current was stopped and a 'wash-out' period of 2 min was allowed. The laser stimulation was then repeated. At the end of the recording and stimulation trials, neurons were labeled with neurobiotin as previously described. Only immunohistochemically identified neurons were used.

Electrical stimulation. In a subset of animals, a bipolar concentric electrode was implanted into the PPN (tip diameters 100 μm and an impedance of ~10 kΩ). Following the baseline recording of VTA neurons, electrical stimulation (0.5-ms duration, 0.5–0.8-mA amplitude) was delivered at 0.5 Hz using a constant-current isolator (A360D, World Precision Instruments). Neurons were subsequently labeled as previously described. Only immunohistochemically identified neurons were used.

***In vitro* recordings.** Male adult mice aged 2–4 months (on a 12-h light cycle, group housed and with free access to food and water) were deeply anesthetized with 100 mg/kg ketamine and then transcardially perfused with ice cold *N*-methyl D-glucamine (NMDG)-based solution containing (in mM): 103.0 NMDG, 2.5 KCl, 1.2 NaH_2PO_4, 30.0 $NaHCO_3$, 20.0 HEPES, 25.0 Glucose, 101.0 HCl, 10.0 $MgSO_4$, 2.0 Thiourea, 3.0 sodium pyruvate, 12.0 *N*-acetyl cysteine, 0.5 $CaCl_2$ (saturated with 95% O_2 and 5% CO_2, pH 7.2–7.4). After decapitation, the brain was quickly removed and transferred into a beaker containing the ice-cold oxygenated NMDG-based solution. Parasagittal sections containing VTA, 300 μm in thickness, were cut in the same medium using a Vibratome 3000 and immediately transferred to recover in well oxygenated NMDG-based solution at 35 °C for 5 min, after which they were transferred to well-oxygenated normal Ringer's solution at 25 °C until placed in the recording chamber constantly perfused (2–4 ml/min) with oxygenated Ringer's solution at 32–34 °C.

Slices were visualized under light illumination with a high-sensitivity digital frame transfer camera (Cooke SensiCam) mounted on an Olympus BX50-WI microscope with a 40× long working distance water-immersion lens. Visualization was achieved using infrared–differential interference contrast microscopy. Micropipettes for whole-cell recording were constructed from 1.2-mm outer diameter borosilicate pipettes on a Narishige PP-83 vertical puller. The standard internal solution for whole-cell current-clamp recording was as follows (in mM): 130 potassium gluconate, 10 KCl, 2 $MgCl_2$, 10 HEPES, 4 Na_2ATP, 0.4 Na_2GTP, pH 7.3, 1% biocytin. The pipettes had a DC impedance of 3–5 MΩ. Membrane currents and potentials were recorded using an Axoclamp 700B amplifier (Molecular Devices). Recordings were digitized at 20–40 kHz with a CED Micro 1401 Mk II and a PC running Signal, version 4 (Cambridge Electronic Design). Drugs were applied in the perfusion medium or locally via a micropipette using a Picospritzer (General Valve), at 20 psi/25 ms, at 0.05 Hz. Carbamylcholine chloride (carbachol, 200 μM), mecamylamine hydrochloride (MEC, 5 μM), dihydro-b-erythroidine hydrobromide (DHβE, 1μM), methyllycaconitine citrate (MLA, 500 nM), bicuculline (10 μM), 6-cyano-7-nitroquinoxaline-2,3-dione (CNQX, 10 μM) and 2[R]-amino-5-phosphonovaleric acid (AP5, 10 μM) were purchased from Tocris. All drugs were dissolved freshly in Ringer's solution. Sections with the recorded neurons were incubated with antibodies against TH as described above and visualized under a confocal microscope. Numerical values in the data are represented as mean value ± s.e.m. Data were analyzed using paired two-tailed *t* test with Origin Pro 7 software. Differences were considered to be significant at $P < 0.05$.

Immunohistochemistry and Image Processing. Sagittal sections of the right hemispheres were cut at 50-μm thickness using a vibratome (VT1000S, Leica). Sections at the approximate levels of the NAcc, PPN, LDT and VTA were collected in 24-well plates. They were incubated in a blocking solution consisting of 10% normal donkey serum (NDS) in PBS containing 1% Triton X-100 for a minimum of 1 h. All primary antibodies used below have been previously validated.

The sections containing the retrograde tracers injected in the VTA were first processed to identify the injection sites. Only those cases where the injections were contained within the borders of the rostral or caudal VTA were included in the study ($n = 4$ rats). Sections containing the PPN and LDT at three different mediolateral levels (two of which contained both nuclei) were incubated with an antibody against choline acetyltransferase (ChAT; raised in goat; 1:500 dilution in 1% NDS, 0.03% Triton X-100 in PBS, Millipore AB144P) and an antibody against CTb (raised in mouse; 1:1,000 dilution in 1% NDS, 0.03% Triton X-100 in PBS, Abcam ab35988) followed by several washes in PBS and incubation in a CY5-conjugated donkey anti-goat antibody (1:1,000, Jackson Immunoresearch 705-175-147) and an Alexa488-conjugated donkey anti-mouse antibody (1:1,000 dilution, Jackson Immunoresearch 715-225-150). Neurons containing RB-R did not require any further processing. The sections were mounted on slides in VectaShield and examined under a fluorescent microscope (ImagerM2, Zeiss, Carl Zeiss AG) using the following filters (nm): 504 for CTb-Alexa488, 560 for RB-R and 650 for ChAT-CY5. Multi-channel stacks of images were taken in the Z plane using a digital camera (Hamamatsu ORCA-ER digital Camera, Hamamatsu Photonics K.K) in combination with the acquisition software, Axiovision 4.8.1 (Carl Zeiss AG). The brightness and contrast of the images were subsequently adjusted in Photoshop (Adobe Systems). The distribution of labeled neurons was digitized off-line using StereoInvestigator (Micro Bright Field, MBF Biosciences) and each was assigned a category depending on the markers expressed. The number of neurons positive for each marker was then quantified as described below.

For the evaluation of the transduction of cholinergic neurons in the PPN/LDT and axons in the VTA, sections were incubated with an antibody against GFP (1:1,000, raised in rabbit, Invitrogen, A21311) and either an antibody against ChAT (to label PPN/LDT somata; details as above) or against tyrosine hydroxylase (TH; to define the VTA borders; raised in chicken; 1:500 dilution in 1% NDS, 0.03% Triton X-100 in PBS, Abcam 76442). To determine the proportion of cholinergic neurons transduced, multi-channel stacks were acquired (as described above) and analyzed off-line using StereoInvestigator.

For detecting the presence of vesicular transporters in PPN/LDT axons in the VTA, sections were incubated with antibodies against the vesicular acetylcholine transporter (VAChT, 1:500, raised in guinea pig, Millipore, ABN100) or the vesicular glutamate transporter-2 (VGluT2, 1:500, raised in rabbit, Life Technologies, 42-7800), in combination with antibodies against GFP and TH, as described above). Fluorescent images were obtained with a confocal microscope (LSM-510, Zeiss) using the following filters: 504 nm for Alexa Fluor-488, 560 nm for CY3 and 650 nm for CY5 (40×, 1.4 numerical aperture oil immersion). Confocal images were processed using Huygens Professional deconvolution software (version 4.1; Scientific Volume Imaging) with a maximum of 40 iterations.

The sections containing juxtacellularly-labeled VTA neurons were incubated in CY3-streptavidin solution (1:1,000, Gelifsciences, PA43001) in PBS, containing 0.03% Triton for a minimum of 4 h. They were then examined under a fluorescent microscope using a 560-nm filter and those sections containing labeled neurons were incubated overnight with the chicken anti-TH, followed by several washes in PBS and incubation with a CY5-conjugated donkey anti-chicken antibody (1:1,000, Jackson Immunoresearch, 703-175-155). Streptavidin-positive neurons (that is, neurobiotin-labeled) that were TH-immunopositive were processed further. The presence of FG in labeled neurons was evaluated using an ultraviolet filter (450 nm), which revealed a strong signal in the somata of retrogradely labeled neurons. Images of triple-positive neurons (streptavidin-CY3, TH-CY-5 and FG) were captured using a fluorescent microscope and Axiovision software. FG-negative neurons were then incubated overnight with an antibody against CTb (as above) followed by several washes in PBS and incubation with an AMCA-conjugated donkey anti-mouse antibody (1:1,000 dilution, Jackson Immunoresearch, 715-155-151). Images of triple-positive neurons (streptavidin-CY3, TH-CY-5 and CTb-AMCA) were captured as above.

In addition to the analysis of VTA sections containing labeled neurons, all brains were also processed to confirm the sites of injection of the retrograde tracer in the NAcc and the transduction sites (in PPN or LDT). Thus, sections were examined by fluorescent microscopy to identify the FG deposit, the CTb deposit (following immunohistochemical processing as described above) and the hChR2-YFP signal. If tracers were off target, the recorded and juxtacellularly labeled neurons were still included in the analysis, but the retrograde labeling was not taken into consideration. If the transduction was weak or overlapped between the two cholinergic nuclei, the neurons were excluded.

© 2016 Nature America, Inc. All rights reserved.
npg

Preparation of tissue and immunohistochemistry for electron microscopy. Sections from ChAT::Cre$^+$ rats were incubated in a cryoprotectant solution (0.05 M phosphate buffer, 25% sucrose, 10% glycerol) overnight, then freeze-thawed in order to increase penetration of the reagents. Sections were double-immunolabeled to reveal postsynaptic TH-containing structures using an anti-TH antibody and presynaptic YFP-containing axons using a biotinylated antibody against GFP (see details below). Normal goat serum in PBS was used to block (10% NGS) sections before the addition of primary antibodies. All sections were first incubated for 24 h at 22–24 °C in mouse monoclonal antibody against TH (1:1000; Sigma T2928). Sections were then incubated for 2–4 h in anti-mouse gold-conjugated antibody (1:200; 1.4 nm colloidal gold, #2001, Nanoprobes). This was followed by washes in PBS and acetate buffer (0.1 M sodium acetate 3-hydrate, pH 7.0–7.5) in preparation for silver intensification of the conjugated gold particles. Silver reagent (HQ Silver kit, #2012, Nanoprobes) was added to each section and allowed to react for 5 min. After washing thoroughly, the sections were incubated in a biotinylated antibody against GFP, raised in goat (1:500; Vector, BA-0702) overnight at 22–24 °C. This was followed by incubation in an avidin-biotin-peroxidase complex (ABC Elite, 1:100; PK6100, Vector) for 3–4 h at 22–24 °C. After washing, the sections were incubated in Tris-buffer (0.5 M, pH 8; TB) containing 0.025% diaminobenzidine solution (DAB wt/vol, Sigma) and 0.5% nickel ammonium sulfate (wt/vol, Sigma) for 15 min. The peroxidase reaction was initiated by the addition of H_2O_2 to a final concentration of 0.01% and allowed to continue for 7–10 min. The sections were postfixed in 1% osmium tetroxide in PB for 12 min, dehydrated, infiltrated with resin (Durcupan ACM, Fluka), mounted on slides and cured at 60 °C for 48 h.

Electron microscope analysis. All sections were examined in the light microscope to determine the extent and localization of the labeling within the limits of the VTA. The selected regions were cut from the slides and re-embedded for ultrathin sectioning for the electron microscope. Serial sections (~50 nm, at least six per grid) were cut on an ultramicrotome (Leica Microsystems, EM UC6), collected on pioloform-coated single-slot grids and lead-stained for 5–7 min. Sections were examined in a Philips CM100 electron microscope. All analyses were performed at a minimum of 5 µm from the tissue-resin border (that is, the surface of the section). The maximum distance from the tissue-resin border examined was determined by the penetration of the gold conjugated antibody together with the angle at which the tissue-resin was sectioned, and was therefore variable.

YFP-positive axonal profiles were identified by the peroxidase reaction product and examined in serial sections. Synapses were identified (n = 10 synapses for PPN; n = 11 synapses for LDT) and their postsynaptic targets were characterized as TH immunopositive (five or more immunogold particles) or immunonegative over six serial sections. Synapses of the asymmetrical type (Gray's type 1) were characterized as such by the presence of presynaptic vesicle accumulation, a thick postsynaptic density, a widened synaptic cleft and cleft material, whereas symmetric synapses (Gray's type 2) possessed a much less pronounced postsynaptic density. The digital images were analyzed using ImageJ, and they were adjusted for contrast and brightness using Adobe Photoshop CS5.1.

Analysis of connectivity. The distribution and numbers of neurons projecting to the rostral and caudal VTA were recorded to identify the topographical relationships between the VTA and brainstem. Neurons in the PPN (n = 3 rats) and LDT (n = 3 rats), as delimited by the ChAT-immunopositive cell bodies, were classified as ChAT$^+$/CTb$^+$, ChAT$^+$/RB-R$^+$, ChAT$^-$/CTb$^+$ or ChAT$^-$/RB-R$^+$. Three representative mediolateral levels were selected for the analysis, corresponding to the following levels from the midline: 1.13, 1.55 and 1.9 mm (ref. 55). To determine the rostrocaudal distribution, VTA-projecting neurons were analyzed using an adaptation of a method based upon the subdivision of the PPN into equally spaced segments, as described previously[56]. Using the center of the substantia nigra pars reticulata (SNr) as a reference point, concentric circles at 300 µm intervals were drawn outwards to cover the entire extent of the PPN; the first two segments covered the SNr and marked the most rostral border of the PPN. From this border, and using the concentric circles, the PPN was divided into three equally-sized segments of 900 µm each along its rostro-caudal axis, representing the rostral (S-I; 0.6–1.5 mm from the SNr), middle (S-II; 1.5–2.4 mm) and caudal (S-III; 2.4–3.3 mm) PPN, from lateral to medial sections. LDT neurons were quantified in a single segment. Results are expressed as the total number of neurons in each category, and as the percentage of cholinergic neurons expressing one of the tracers, using the mediolateral levels or rostrocaudal segments to average across all animals. We used a Wilcoxon signed-rank test to compare differences (the data was not normally distributed).

For the analysis of the cholinergic innervation of the VTA, we measured the length of axons of cholinergic neurons transduced in the PPN (n = 3 rats) and LDT (n = 3 rats) as an estimate of density of innervation. In order to obtain a reliable comparison between the innervation of each structure, we analyzed the density of axons following transduction using only the AAV2-EF1a-DIO-eYFP, thus avoiding confounding factors such as possible differences in the efficiency of the vector to transduce cholinergic neurons or differences in the strength of the fluorescent signal. In each case, the location of the transduction area was confirmed to be contained in the limits of the PPN or the LDT. Images were acquired using a 5× magnification objective for delimiting the border of the VTA defined by TH-immunolabeling, and 20× for detecting fluorescent axons. For each brain, three sections corresponding to approximately 0.4, 0.9 and 1.4 mm from the midline[55] were analyzed. A grid of 250-µm^2 squares was superimposed and in each square the total length of labeled axons was measured by tracing all fluorescent axons using in-built Neurolucida functions. The results are expressed as total axonal length in each square (expressed as µm) or as a normalized value for each square relative to the total length in each VTA level (expressed as percentage). Data was then calculated in three dimensions (rostrocaudal, mediolateral and dorsoventral) in order to identify topographical relationships with the VTA. To identify differences in the axonal length across rostrocaudal segments, we used an ANOVA on ranks analysis (the data was not normally distributed), and to compare between the axonal length at specific segments between PPN and LDT axons, we used an unpaired t test. The level of significance for all tests was taken to be $P < 0.05$. Data are expressed as mean ± s.e.m. unless otherwise indicated.

Evaluation of additional cholinergic inputs to the VTA. Sections from brains of ChAT::Cre$^+$ rats that received injections in each brain cholinergic nucleus were analyzed to identify alternative sources of acetylcholine in the VTA that was distinct from the brainstem (Ch5, PPN and Ch6, LDT). Thus, AAV2-EF1a-DIO-eYFP injections were delivered in the following locations and stereotaxic coordinates (from bregma, in mm; DV ventral to the dura): Ch1 (medial septum) AP: +0.7, ML: 0.2, DV: 4.5; Ch2 (vertical limb of the diagonal band of Broca) AP: +0.5, ML: 0.4, DV: 7.5; Ch3 (horizontal limb of the diagonal band of Broca) AP: +0.1, ML: 1.6, DV: 8.5; Ch4 (nucleus basalis of Meynert) AP: +0.9, ML: 2.5, DV: 7.0; Ch7 (medial habenula) AP: −3.5, ML: 0.3, DV: 4.0; and Ch8 (parabigeminal nucleus) AP: −4.5, ML: 4.3, DV: 5.5, as described previously[57]. Sections containing the VTA were selected and incubated to reveal TH and YFP immunoreactivities as described above. The processed sections were mounted on slides using Vectashield and then examined under a confocal microscope, as above. The border of the VTA was delimited by the TH immunostaining and carefully scanned for YFP-positive labeled axons. No YFP-labeled axons were detected within the VTA following injections in any cholinergic cell group other than the PPN or LDT.

Electrophysiological data analysis. Following histological confirmation of their location and neurochemical nature, the recordings of VTA neurons were analyzed to determine their basic electrophysiological properties. Spike trains were digitized and converted into a time series of events using in-built Spike2 functions. The baseline activity, firing patterns and action potential duration were determined from 5 min-long initial recordings. To determine variations in the firing rate following experimental manipulations, 20 s segments of baseline activity preceding the manipulation were compared to the firing rate during the pinch or laser stimulation and expressed as percentage change.

The responsiveness of neurons was determined by computing a time-resolved average response to light stimulation. For this, 2 to 4 trials for each neuron were obtained and a modified estimation of the mean instantaneous firing rate locked to the onset of the laser was computed[58]. By considering each spike train j = 1, …, k as a sequence of discrete events with occurring times $\{t_{i,j}\}$, I = 1, 2, …, n_j, a cumulative distribution function (CDF) at each time $t_{i,j}$ can be defined. The number of events before and up to $t_{i,j}$ is a strictly increasing step function changing at $t_{i,j}$ in unit steps. The slope of CDF divided by the number of trials represents the mean density of events across the k trials and is equal to the mean density of events per unit time or the trial-averaged firing rate. Then a local linear

© 2016 Nature America, Inc. All rights reserved.
npg

doi:10.1038/nn.4335

regression based on $N_{i,j} = 6 \times k$ neighboring events may be used to estimate the CDF slope for each spike time and the regression slope estimates the instantaneous firing rate at each reference time $t_{i,j}$ while considering the response of the k trials. Finally, an evenly sampled time series $FR(t)$ was obtained by smoothing the resulting (unevenly-sampled) time series with a 1 s Gaussian kernel. The distribution $FR(t)$ of spontaneous activity before the stimulus was then used to compare the activity during laser application with the basal activity. Percentiles 5 (C_5) and 95 (C_{95}) of the $FR(t)$ during the pre-stimulus period were selected as thresholds to assess inhibition and excitation in the post-stimulus interval respectively. Significance of response periods was assessed by means of a cluster-based permutation test ($n = 200$ permutations, $P < 0.05$) on the duration of the intervals. If a neuron showed a post-laser period with $FR(t)$ above percentile 95 or below percentile 5 for a longer period than any other within the baseline (and not less than 3 s), then the neuron was considered to respond to cholinergic axon activation either by excitation or inhibition. If these criteria were not met then a neuron was considered as non-responding. Cluster-based permutation tests ($P < 0.05$, $n = 200$ permutations) were used to assess differences in the response of LDT or PPN axon stimulation in NAcc-projecting neurons[59]. Data are depicted as mean ± 95% CI.

Neurons that were classified as regular (only for descriptive purposes) showed more than three spaced peaks in their autocorrelogram. To determine bursting activity, typical parameters for DA neurons were used where the burst onset was defined by a minimum of two events with an interval of 80 ms or less, and the burst termination was determined if the interval between events was larger than 160 ms (ref. 60). The number and characteristics of the bursts were analyzed using Spike2 scripts (Cambridge Electronic Design), including the number and percentage of spikes inside bursts, the number and percentage of inter-burst spikes and the burst probability (normalized burst count difference between basal and laser stimulation). Two-tailed Student's t test (t) (unless otherwise stated) and analysis of variance (ANOVA, F) were used to compare normally distributed data between groups; Mann-Whitney Rank Sum Test (U) was used when data failed normality. Linear regressions were used to compare the firing rate changes between different modalities of experimental manipulations (that is, laser versus pinch), calculating the Studentized Deleted Residuals to detect outliers (SigmaPlot 12.0, Systat Software, Germany). The significance level for all tests was taken to be $P < 0.05$. Data are expressed as mean ± s.e.m.

Behavioral evaluation. 2 weeks following the injection of AAV2-EF1a-DIO-hChR2-eYFP in the PPN ($n = 12$ rats) or LDT ($n = 10$ rats) of ChAT::Cre$^+$ and WT ($n = 10$ rats) animals, an optic fiber was implanted in the VTA. Animals were anesthetized and the skull exposed as previously described. Six stainless-steel anchoring screws (Morris Co.) were fixed to the skull. A custom-made 200-µm-diameter optic fiber (flat-cut, multimode, 0.39 NA, 8 mm long; Thorlabs) connected to a SMA-905 connector was slowly lowered up to 200 µm above the right VTA (AP: −6.2 mm, ML: 0.9 mm, DV: 7.3 mm from the brain surface, relative to Bregma) and kept in position with light curing dental cement (Flowable Composite, Henry Schein). The connector was kept protected by a dust cap (CPAMM SMA905, Thorlabs) and replaced daily until completing the experiments. Animals received 5 d of non-steroidal anti-inflammatory (Carprieve, 5 mg/kg; s.c.; Norbrook Laboratoris) and antibiotic (Baytril, 2.5%, 0.5 ml/kg, s.c., Bayer) treatment before the behavioral testing. Animals were handled daily and were caged in pairs. Before implantation and after perfusion, the power in the laser output at the tip of the optic fiber was tested. Any optic fiber unable to deliver a minimum of 5 mW was excluded.

During all operant behavioral experiments, animals were food-deprived, receiving free access to food for 4 h per d (LabDiet) to maintain 85% of their starting weight. All behavioral experiments were performed during the active (dark) phase. Two days before initiation of the training, each animal received in their home cage, 0.5 g of sugar pellets (Dustless precision sugar pellet, 45 mg, BioServ). 1 d before initiation of training, they were individually placed in operant boxes (Med Associates) where 20 pellets were randomly delivered in the food magazine during a 20-min period in order to habituate animals to the magazine and food delivery. On the opposite wall to the magazine, a house light (3 W, 24 V) and a fan (Med Associates) were turned on during all experiments. Operant boxes were individually placed in sound attenuated cubicles (Med Associates). At the end of the 20-min session, the house light was turned off for 5 min before the animal was removed from the box. This step was repeated until the animal ate the 20 pellets in the 25-min period. The order in which the animals were tested was kept constant during all experiments; each operant chamber was deeply cleaned between animals. Levers were placed in either side of the magazine. Animals were then manually trained in a continuous reinforcement (CRF) schedule (fixed ratio 1, 1 ms delay for food delivery) where every lever press was reinforced by a single sugar pellet. To facilitate acquisition, an LED (ENV-229M, Med Associates) was placed above the magazine and turned on for 8 s following each sugar pellet delivery. Animals were kept on CRF until they autonomously completed 80 presses in a 30-min session over two consecutive days. Next, animals underwent 2 d of VI15 (variable interval; reinforcements follow the first press after 15-s average intervals, 30-min duration), followed by 2 d of VI30 (reinforcements follow the first press after 30-s average intervals, 30-min duration). Following the second session of VI30 (VI30-2), animals were transferred to the optical stimulation chamber (similar boxes as previously described but the roof of the box was removed, Med Associated Inc.) and habituated to an optic fiber patch cord during the session. They then underwent VI30-3 schedules until they recovered at least 80% of the total press in VI30-2. Reinforcer devaluation (extinction) occurred over 4 consecutive days (ext1 to ext4). A blue laser (same as above) was connected to the optic fiber patch cord using an intermediary single rotary joint (FRJ, Doric lenses). Laser power was adjusted for every animal in order to deliver a power of 5 mW at the tip of the fiber. During extinction, the rats were tested in a VI30 session where lever presses were recorded but reinforcer delivery was replaced by laser stimulation (8-s pulses, 10 Hz, 50 ms on/off, controlled by 28 V DC to TTL Adaptor, product number SG-231, Med Associates). The minimum interval between laser stimulations was 9 s. For all sessions (CRF1 to ext4), lever presses, magazine entries, reward deliveries, laser stimulation and pellet collection latencies were recorded in real time using Med-PC software (Med Associates).

The animals were then evaluated in open field over 3 consecutive days. They were placed into a dark, custom-made open field box (50 cm × 50 cm × 50 cm). Light was adjusted to 15 lx using multiple red light sources (60 W) with the box being deeply cleaned between animals. Motor activity was monitored over 30 min using AnyMaze software (Anymaze technology SA) using a high-resolution camera (C615, Logitech) positioned vertically to the box. Distance traveled was recorded in 1-s bins. On the first day, animals were habituated to the open field (no stimulation was delivered). On the second and third days, rats received optogenetic stimulation as above (train pulses were delivered every 2 min), but 30 min before testing they received either a saline injection (i.p., 0.3 ml) or a cholinergic antagonist cocktail (i.p., 0.3 ml final volume in 0.9% saline; MLA: 6 mg/kg; DHβE: 3 mg/kg; atropine: 0.5 mg/kg; mecamylamine: 1.0 mg/kg).

Behavioral analysis. Differences in the cumulative distance traveled by the animals under the effect of optogenetic stimulation in PPN, LDT and control groups were evaluated. A non-parametric cluster-based test was used to compare the cumulative distance in 5-s windows ($P < 0.05$). Clusters with less than 10 s were considered as non-significant. The stimulation-locked effects on locomotion were analyzed by comparing the locomotor activity before, during and after stimulation with a 1-s resolution. The mean and s.d. were obtained from the 10-s period before the stimulation (pooling all the pre-stimulation periods across the whole set of trials). These parameters served to normalize the activity of the animals in each stimulation trial (13 trials per rat). Trial-related activity was then averaged to extract an average estimate of locomotion for each animal. Significant changes in the activity during and after the stimulation across rats were assessed by means of a paired non-parametric cluster-based test comparing post/during activity with that of the pre-stimulation period. Data from lever presses were analyzed using one-way ANOVA and two-way ANOVA with Tukey *post hoc* tests. ANOVA analyses were performed using SPSS (SPSS statistic software, IBM).

Technical considerations. Our results show that cholinergic neurons of the brainstem modulate specific subsets of DA and non-DA neurons in the VTA. The accurate dissection of these pathways primarily relied on the detection of retrogradely-labeled neurons in the VTA and the anatomical specificity of the transductions in the brainstem. In order to identify mesolimbic neurons, we injected commonly used retrograde tracers (Fluorogold or cholera toxin-B; alternated between animals) in the lateral shell of the NAcc. Retrogradely-labeled mesolimbic neurons were detected predominantly in the dorsal part of the VTA, in agreement with previous studies[25,61]. Although the distribution of labeled

© 2016 Nature America, Inc. All rights reserved.

neurons remained constant across animals, the number of labeled neurons varied. This suggests a variable number of false-negative neurons in each animal (that is, mesolimbic neurons that were not labeled by the tracer). Because we used the retrograde labeling to compare the influence of PPN and LDT over identified mesolimbic neurons, the presence of false-negative neurons is unlikely to affect the interpretation of our results. To prevent misclassification of non-labeled neurons, we have not considered them as a single, homogeneous group.

The second critical factor to ensure the accurate dissection of the connectivity between neuronal subsets was the anatomical specificity of the PPN and LDT transductions. Both cholinergic structures are located in the dorsal and caudal brainstem and there are no clear boundaries that separate them. While the core of the caudal PPN shows higher density of cholinergic neurons, the density diminishes toward its caudal pole; this region of low density of cholinergic neurons marks the transition between PPN and LDT and is sometimes referred to as the subpeduncular tegmental nucleus. The LDT, situated more medially and caudally to the posterior pole of the PPN, is characterized by an area with a high density of cholinergic neurons[62]. We thus used the area of low cholinergic neuron density to distinguish between caudal PPN and LDT. Small volumes of the viral vectors were injected to ensure the anatomical specificity, and only injections restricted to these areas were considered further. Our analysis of the transduction areas did not reveal overlap in the fluorescent signal between the two nuclei.

The low volume injections into the PPN and LDT that were used to ensure anatomical specificity produced restricted transduction that did not cover the entire caudal PPN or LDT. Furthermore, we observed a transduction rate of about 60% of cholinergic neurons within the injection area in the PPN and LDT (**Supplementary Table 2**). This means that the number of cholinergic neurons transduced with ChR2, and hence their axons in the VTA, do not represent the entire brainstem cholinergic innervation of the VTA. Such variability in the transduction is likely to be reflected in the frequency and magnitude of the effects observed in DA and non-DA neurons following optogenetic activation of cholinergic axons. In other words, our results are likely to be an underestimate of the magnitude of the cholinergic drive in the VTA and may explain why 30–40% of DA neurons did not respond to the stimulation. This idea is supported by the fact that more than 90% of DA neurons express muscarinic and nicotinic receptors[63–66]. Furthermore, in our whole-cell slice recordings, we observed responses to carbachol in all DA neurons sampled. Thus, although our experimental approach was able to characterize the effects of cholinergic signaling in the VTA at the single-cell level, it may be underestimating the effects at the circuit level.

Statistical methods. Statistical comparisons were performed using Origin Pro 7 (OriginLab), SigmaPlot 12.0 (Systat Software), SPSS (IBM SPSS) and Matlab (Mathworks) software. Specific statistical tests are explicitly stated in the corresponding methods sections above. When needed, data was formally tested for normality. If the data passed the normality test, parametric statistics were used. If failed, non-parametric test was chosen. No statistical methods were used to predetermine sample sizes. Sample size was decided on the basis of our previous experience in the field and was not pre-determined by a sample size calculation. The sample size are similar to those generally employed in the field and is justified by the high rate of exclusion due to the difficulty of the combined methodological approaches (site of injection, labeling of the neurons, location of the neurons, etc.).

No randomization was used for electrophysiology or anatomy. For behavior, operant boxes, testing order and drugs order were randomized using unbiased simple randomization. No blinding was performed for experimental groups, data analysis or behavioral testing; nevertheless, neurons were sampled without distinction of their firing properties or stereotaxic coordinates within the VTA, and the neurochemical identity was revealed *post hoc*.

Neurons were excluded from the analysis if their location was out of the VTA, their location did not match the stereotaxic coordinates during the recording, their neurochemical identity could not be verified or the virus infection in the brainstem was not successful.

A **Supplementary Methods Checklist** is available.

Data availability. The data that support the findings of this study and the custom Matlab code are available from corresponding author on request.

51. Mena-Segovia, J., Sims, H.M., Magill, P.J. & Bolam, J.P. Cholinergic brainstem neurons modulate cortical gamma activity during slow oscillations. *J. Physiol. (Lond.)* **586**, 2947–2960 (2008).
52. Pinault, D. A novel single-cell staining procedure performed *in vivo* under electrophysiological control: morpho-functional features of juxtacellularly labeled thalamic cells and other central neurons with biocytin or Neurobiotin. *J. Neurosci. Methods* **65**, 113–136 (1996).
53. Thiele, A., Delicato, L.S., Roberts, M.J. & Gieselmann, M.A. A novel electrode-pipette design for simultaneous recording of extracellular spikes and iontophoretic drug application in awake behaving monkeys. *J. Neurosci. Methods* **158**, 207–211 (2006).
54. Herrero, J.L. *et al.* Acetylcholine contributes through muscarinic receptors to attentional modulation in V1. *Nature* **454**, 1110–1114 (2008).
55. Paxinos, G. & Watson, C. *The Rat Brain in Stereotaxic Coordinates* (Academic Press, San Diego, 1986).
56. Mena-Segovia, J., Micklem, B.R., Nair-Roberts, R.G., Ungless, M.A. & Bolam, J.P. GABAergic neuron distribution in the pedunculopontine nucleus defines functional subterritories. *J. Comp. Neurol.* **515**, 397–408 (2009).
57. Dautan, D., Hacioğlu Bay, H., Bolam, J.P., Gerdjikov, T.V. & Mena-Segovia, J. Extrinsic sources of cholinergic innervation of the striatal complex: a whole-brain mapping analysis. *Front. Neuroanat.* **10**, 1 (2016).
58. Blejec, A. Statistical method for detection of firing rate changes in spontaneously active neurons. *Neurocomputing* **65**, 557–563 (2005).
59. Maris, E. & Oostenveld, R. Nonparametric statistical testing of EEG- and MEG-data. *J. Neurosci. Methods* **164**, 177–190 (2007).
60. Grace, A.A. & Bunney, B.S. The control of firing pattern in nigral dopamine neurons: single spike firing. *J. Neurosci.* **4**, 2866–2876 (1984).
61. Swanson, L.W. The projections of the ventral tegmental area and adjacent regions: a combined fluorescent retrograde tracer and immunofluorescence study in the rat. *Brain Res. Bull.* **9**, 321–353 (1982).
62. Mena-Segovia, J. Structural and functional considerations of the cholinergic brainstem. *J. Neural Transm. (Vienna)* (in the press) (2016).
63. Garzón, M. & Pickel, V.M. Subcellular distribution of M2 muscarinic receptors in relation to dopaminergic neurons of the rat ventral tegmental area. *J. Comp. Neurol.* **498**, 821–839 (2006).
64. Garzón, M. & Pickel, V.M. Somatodendritic targeting of M5 muscarinic receptor in the rat ventral tegmental area: implications for mesolimbic dopamine transmission. *J. Comp. Neurol.* **521**, 2927–2946 (2013).
65. Azam, L., Winzer-Serhan, U.H., Chen, Y. & Leslie, F.M. Expression of neuronal nicotinic acetylcholine receptor subunit mRNAs within midbrain dopamine neurons. *J. Comp. Neurol.* **444**, 260–274 (2002).
66. Faure, P., Tolu, S., Valverde, S. & Naudé, J. Role of nicotinic acetylcholine receptors in regulating dopamine neuron activity. *Neuroscience* **282C**, 86–100 (2014).

© 2016 Nature America, Inc. All rights reserved.